

## Chapter 2

# Carbon Nanowalls: A Potential 2-Dimensional Material for Field Emission and Energy-Related Applications

Sanjay Kumar Srivastava, Vikram Kumar and V.D. Vankar

**Abstract** Carbon, an abundant material in the earth crust, is also the most attracting, in particular, owing to variety of fascinating materials it forms. It can appear as a transparent crystal (such as diamond), but also as black amorphous soot. It is associated with a rich and diverse chemistry. Carbon materials, in general, can be classified into different dimensional categories such as three-dimensional (3-D), two-dimensional (2-D), one-dimensional (1-D), and zero-dimensional (0-D) depending on the relative sizes in different spatial directions. Fullerenes are 0-D whereas carbon nanotubes (CNTs), nanofibres, or nanorods are 1-D nanostructures. Graphite nanosheets or nanowalls are considered as 2-D structures. A great attention has been given to the 0-D and 1-D carbon nanostructures, but studies on the growth and the properties of 2-D carbon nanowalls (CNWs) are not so abundant as in the case of fullerene or CNTs. The CNWs are very promising class of 2-D nanomaterials since the CNWs are characterized by an open boundary structure. On the other hand, fullerene and CNTs are closed boundary structures. Each CNW is made of several graphene sheets stacked over each other. The CNWs have a large surface area, which makes them very attractive for various potential applications such as chemical and biosensors or energy storage devices. Moreover, the CNWs have sharp edges normal to the substrate which make them very useful for field emission applications. In this chapter, growth of CNWs by various methods is discussed with an emphasis on plasma-enhanced chemical vapor deposition (PECVD) method. This is followed by the morphological and structural characterization of the CNWs by different techniques. The formation mechanism of CNWs will be described. In addition, properties of CNWs in respect to their

---

S.K. Srivastava (✉)

CSIR-National Physical Laboratory, New Delhi 110012, India

e-mail: srivassk@nplindia.org; sksrivastava78@gmail.com

S.K. Srivastava

Academy of Scientific & Innovative Research (AcSIR),

CSIR-NPL Campus, New Delhi 110012, India

V. Kumar · V.D. Vankar

Department of Physics, Indian Institute of Technology Delhi,

Hauz Khas, New Delhi 110016, India

potential applications in field emission and energy related devices including lithium ion batteries, fuel cells and solar cells, is also reviewed in the light of their unique morphology and structure.

## 2.1 Introduction

Carbon, which is abundantly found in the earth crust, is the most attracting materials in present era, in particular owing to variety of fascinating materials it forms. It can appear as a transparent crystal (such as diamond), but also as black amorphous soot. It is associated with a rich and diverse chemistry. Prior to 1985, there were only two known crystalline forms of solid carbon: diamond and graphite. The discovery of buckminsterfullerene ( $C_{60}$ ) by Kroto et al. [1] followed by its macroscopic synthesis by Krätschmer [2] gave a new direction in the field of carbon research. The subsequent discovery of carbon nanotubes (CNTs) [3] added a new dimension to the knowledge of carbon technology [4].

### 2.1.1 Carbon Nanostructures: An Overview

The synthetic graphite was observed even in the nineteenth century; however, synthetic diamonds were realized only in the later half of the twentieth century. Since then, both graphite- and diamond-related carbon materials have attracted lots of interests in scientific communities. With the discoveries/advancements of new synthesis techniques, these two materials have renewed their importance. In the graphite-based group, new materials such as carbon fibers, glassy carbons, pyrolytic carbon were developed in the early 1960s [5] and found wide commercial applications. The most significant and relatively recent application of this carbon material is in lithium-ion rechargeable batteries, wherein nanostructured carbon-based anodes are used and has lead to feasibility of portable electronic devices [6].

A new era in carbon materials began when the family of buckminsterfullerene ( $C_{60}$ ) [1] was discovered in 1985. Multi-walled carbon nanotubes (MWNTs) were discovered in 1991 by Sumio Iijima of NEC Corporation, Fundamental Research Laboratories, Japan, as a by-product of fullerenes called as helical microtubules of graphite carbon which was produced by arc discharge process [3]. The discovery of these carbon structures lead to a new worldwide research boom that seems still growing with the discovery of exciting materials and their properties. But a fundamental question was prompted that why were CNTs or fullerenes not discovered many years ago? Even all of the techniques required to synthesize and characterize these nanomaterials have been available for decades. In fact, there were evidences for the existence of CNTs before 1991, but they could not be recognized as a new and important form of carbon. The 2-D carbon nanosheets or carbon nanowalls are

relatively new. The 2-D graphite sheets have an open boundary structure whereas fullerene and CNTs have the closed boundary structures. The 2-D CNWs have a much larger surface area as compared to that of fullerene or CNTs which makes them very attractive for chemical, biosensor, and energy storage applications. Moreover, they have sharp edges almost normal to the substrate which could be very useful for field emission applications. Some of the significant developments and discoveries of the nanoscale carbon structures are summarized in Table 2.1.

**Table 2.1** Summary of the developments in the field of carbon nanostructures [6, 7]

Year	Development	Remarks	Reference
1960	Production of carbon tubes with graphite layer structures	Arc discharge method, 5 $\mu\text{m}$ in diameter tubes	Bacon [8]
1966	Theoretical prediction of a large hollow cage molecule	Assumed that the molecule can be fashioned out of graphite	Jones [9]
1970	The soccer ball-shaped $\text{C}_{60}$ molecule is suggested		Osawa [10]
1973	Prediction that $\text{C}_{60}$ would be stable	Huckel calculations, closed shell electronic configuration is predicted	Bochvar and Galperin [11]
1980	First experimental observation of carbon nanotubes by arc discharge process	By high-resolution transmission electron microscopy observation	Iijima [12]
1984	Report on the preferential stability of even-atom carbon cluster especially of a sixty carbon species	Mass spectroscopy study on laser-ablated carbon plumes. Abundance of sixty carbon species in spectrum is reported	Rohlfing et al. [13]
1985	Discovery of $\text{C}_{60}$	$\text{C}_{60}$ and $\text{C}_{70}$ detected in the mass spectrum of laser-evaporated graphite. $\text{C}_{60}$ was named as Buckminsterfullerene	Kroto, Smalley et al. [1]
1990	Mass production of Fullerene	By evaporation of graphite electrodes in an arc discharge process	Kratehmer et al. [2]
1991	Discovery of MWNTs	Observation of helical MWNTs of graphite with closed ends deposited on cathode during the DC arcing of graphite	Iijima [3]
1992	Observation of carbon onions	Spherical shells of graphite obtained by heating of CNTs by the electron beam in a microscope	Ugarte [14]
1992	Mass production of MWNTs	Arc discharge process	Ebbesen and Ajayan [15]
1993	Discovery of SWNTs	By arc process in the presence of catalyst such as Fe or Co	Iijima et al. [16], Bethune et al. [17]

(continued)

**Table 2.1** (continued)

Year	Development	Remarks	Reference
1996	Ropes of SWNTs	By laser ablation method	Smalley et al. [18]
1998	CVD synthesis of aligned MWNT films	By plasma-enhanced hot-filament CVD in the presence of catalyst film	Ren et al. [19]
1998	CVD synthesis of SWNTs	Using catalyst	Kong et al. [20], Hafner et al. [21]
2001	Ordered arrangement of SWNTs	Ordered arrangement of SWNTs of micron size called nanotube single crystals	Schilttler et al. [22]
2002	Growth of carbon nanowalls/nanosheets (CNWs)	By microwave plasma-enhanced CVD method observed especially on insulating substrates coated with NiFe under the influence of intense plasma on the biased substrate CNWs was observed as a by-product of CNTs	Wu et al. [23]
2004	Discovery of graphene-a monolayer of graphite/carbon atoms	Professor Geim and professor Novoselov of University of Manchester, UK, extracted the graphene from a piece of graphite such as is found in ordinary pencils. Using regular adhesive tape, they managed to obtain a flake of carbon with a thickness of just one atom. This was achieved at a time when many believed it was impossible for such thin crystalline materials to be stable.	Novoselov et al. [24]
2010	Nobel Prize in Physics for the year 2010 to Professor Andre Geim and Professor Konstantin Novoselov for their 'groundbreaking experiments regarding the two-dimensional material graphene'		

## 2.1.2 Structural Properties

### 2.1.2.1 Bonding Configuration of Carbon Atoms

In order to understand the structure of carbon nanostructures such as CNTs, graphene, or carbon nanowalls and other related nanostructures, understanding of carbon atoms' bonding structure and properties is essential. A carbon atom has six electrons with electronic configuration  $1s^2, 2s^2, 2p^2$ . The four valence shell

electrons fill the  $sp^3$  or  $sp^2$  and  $sp$  hybrid orbital and are responsible for the different bonding configurations of graphite, diamond, CNTs, fullerenes, or carbon nanowalls. For example, in diamond, four valence electrons of each carbon atom occupy the  $sp^3$  hybrid orbitals and form four equivalent ' $\sigma$ ' covalent bonds to connect four other carbon atoms tetrahedrally and therefore making diamond the hardest known material and electrically insulating [25]. The diamond is transparent in the visible or infrared region, and opaque in the ultraviolet region. It also has high refractive index and unusually high thermal conductivity. Thermodynamically, diamond is metastable at room temperature. In graphite, the three valence electrons of each carbon occupy the planar  $sp^2$  hybridized orbital to form three in-plane  $\sigma$ -bonds and the fourth electron forms an out-of-plane  $\pi$  bond which results in a planar hexagonal network. The hexagonal sheets are held parallel to each other by weak van der Waal's force with an interplanar spacing of 0.34 nm. In  $sp^2$  bonding,  $\sigma$ -bond length and bond energy are 0.14 nm and 420 kcal/mol, respectively, whereas in  $sp^3$  bonding they are 0.15 nm and 360 kcal/mol, respectively. Therefore, graphite is stronger in-plane than diamond. Graphite is stable at room temperature. It is electrically conductive because of the distribution of the out-of-plane  $\pi$  electron over its plane. These loose  $\pi$  electrons' interaction with light causes the graphite optically black. Also, the weak van der Waal's interaction among its parallel sheets makes the material soft because the sheets can easily glided relative to each other and hence making graphite as an ideal lubricant applications [25].

Fullerenes ( $C_{60}$ ) are made by joining 20 hexagons and 12 pentagons made out of carbon atoms forming a spherical shell-like structure. Each carbon atoms in  $C_{60}$  is bonded with three neighboring C atoms in  $sp^2$  bonding configuration. However, there may be small fraction of  $sp^3$  character in these bonds due to the associated curvature. Also, the strain is evenly distributed over the molecule since all the 60 carbon atoms are identical [7].

A carbon nanotube (CNT) is hollow cylinder formed by rolling graphite sheets. Carbon-carbon bonding in CNT is  $sp^2$ . However, circular curvature of the nanotubes may cause rearrangement of  $\sigma$  and  $\pi$  bonding leading to  $\sigma$ - $\pi$  rehybridization, in which three  $\sigma$  bonds are slightly out of plane causing the  $\pi$  orbital to delocalized outside the tube for compensation. This bonding arrangement makes CNTs mechanically stronger, electrically and thermally more conductive, and chemically and biologically more active than graphite. This also causes the incorporation of topological defects into the hexagonal network to form capped, bend, or helical tubes [25]. Based on number of sheets rolled up, nanotubes are classified as single-walled nanotubes (SWNTs) and multi-walled nanotubes (MWNTs). Different allotropes of carbon and their structure are shown in Fig. 2.1.

### 2.1.2.2 Single-Walled Nanotubes

A SWNT is defined as a hollow cylinder of a single graphite sheet. The inner diameter of SWNT is extremely narrow typically 1 nm. SWNTs were discovered in 1993 by arc discharge evaporation method [16, 17]. Generally, SWNTs produced

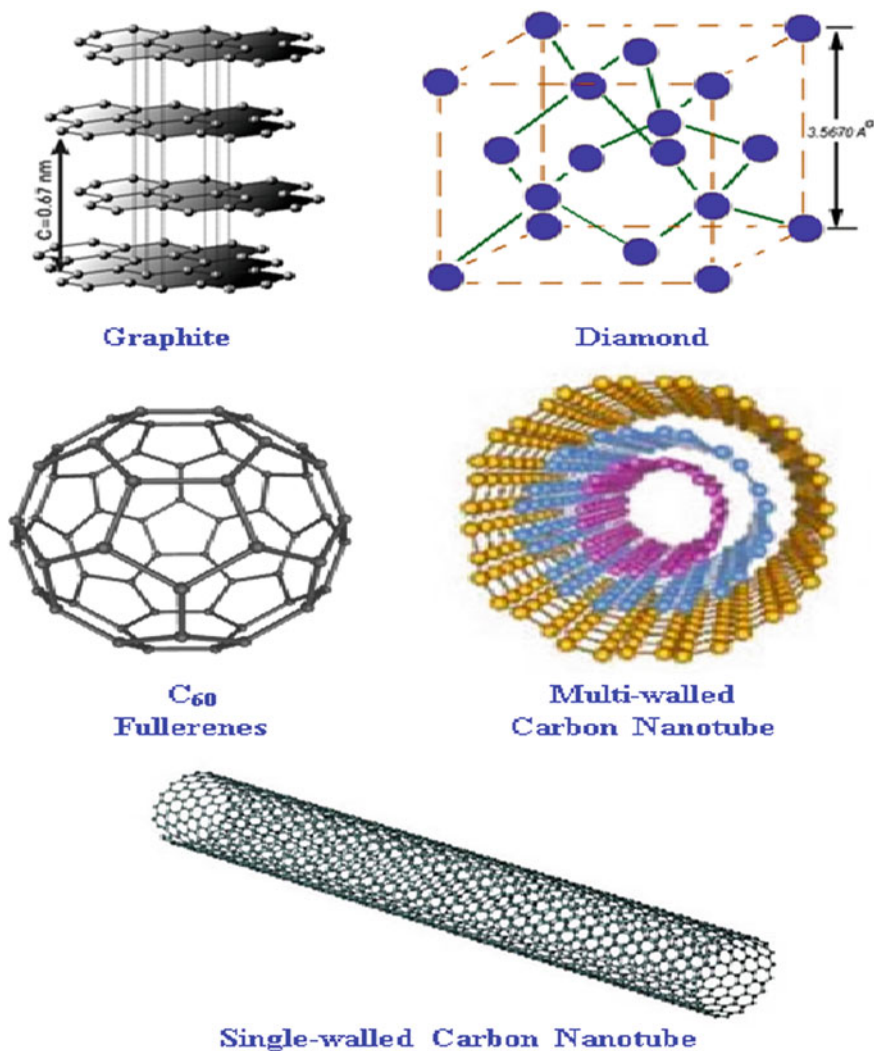


**Fig. 2.1** Different allotropes of carbon and their structure

by conventional arc discharge method are capped. They appear in the form of bundles of tubes or ropes of tubes. The growth of SWNTs is believed to be essentially catalytic. Iron group metals such as iron, nickel, cobalt are used as the catalysts. The catalytically produced SWNTs have a number of interesting features different from those produced by arc evaporation. The catalytic tubes generally have small metal particles attached to one of its ends. The tubes have relatively larger diameters (typically 1–5 nm) dependent on the size of associated catalytic

particle. Also, the catalytically formed SWNTs are generally isolated rather than grouped into bundles as often observed in tubes produced by arc evaporation [26].

### 2.1.2.3 Multi-walled Nanotubes

A MWNT consists of many concentric seamless cylinders or SWNTs. The intertube spacing in MWNTs is typically  $\sim 0.34$  nm which is close to interplanar spacing of (002) planes of graphite. Diameter of MWNTs ranges from 2.5 to 100 nm depending on the process condition used for their synthesis. Figure 2.1 shows the computer generated models of a SWNT and a MWNT. Both the SWNTs and MWNTs have extremely unique structural, mechanical, electrical, electronic, thermal, and field emission properties. However, structure and hence properties of the CNTs are strongly dependent on the synthesis processes.

### 2.1.2.4 Carbon Nanowalls

A thin graphite sheet is a typical example of a 2-D system, whereas a single layer of graphite sheet, otherwise known as 'graphene,' is the most ideal 2-D system [24]. Graphene is a hexagonal arrangement of carbon atoms forming monoatomic planar sheet. It is a promising electronic material due to its high electrical conductivity, chemical and physical stability [27]. In addition, graphene possesses several extraordinary properties such as high ballistic electron mobility ( $>200,000$  cm<sup>2</sup>V<sup>-1</sup>s<sup>-1</sup>) [28], high thermal conductivity (5000 W m<sup>-1</sup>K<sup>-1</sup>) [29], Young's modulus ( $\sim 1150$  GPa), fracture strength (125 GPa) [30], and a high specific surface area ( $\sim 2600$  m<sup>2</sup>g<sup>-1</sup>) [31]. These properties are quite attractive for various applications.

Similar to graphene, the carbon nanowalls (CNWs) is another class of 2-D materials which is described as self-assembled and vertically standing few-layered graphene sheets. These are also called as carbon nanosheets and carbon nanoflakes. The walls are curved and have a height of approximately 1–2  $\mu$ m with average thickness of few to several nanometers. They stand vertically to form a self-supported network structures. As illustrated in Fig. 2.2, each CNW consists of several stacked graphene sheets. CNWs were first reported by Wu et al. in 2002 [23] wherein they observed wall-like carbon nanostructures perpendicular to a substrate and therefore named them as CNWs. Since then, several groups have reported growth of CNWs by different chemical vapor deposition (CVD) methods mainly by plasma-enhanced CVD (PECVD). The CNWs have a high density of atomic-scale graphitic edges normal to the substrates (so-called as nanowalls) that are potential sites for electron field emission. The 2-D CNWs have a large surface area (theoretically twice that of the fullerenes or CNTs) [32] which makes them very attractive for chemical, biosensor, or energy storage applications. Moreover, each CNW has a domain structure which consists of nanographite domains which are several tens of nanometers in size. Such unique morphology and structure of

CNWs have lead to both fundamental as well as applied research. Few of the leading applications of CNWs are as electron field emitters, as the electrodes in lithium-ion batteries, as catalyst supports in fuel cells, and as an electrode or active material in solar cells.

In this chapter, basic properties of CNWs, growth, and their potential applications are described. PECVD due to its relatively low-temperature processing and feasibility for scalability has been one of the most promising techniques for the growth of carbon nanomaterials including aligned or nonaligned CNT films and CNWs. Here, growth of CNWs using microwave plasma-enhanced chemical vapor deposition (MPECVD) is featured. In addition, growth of CNWs by inductively coupled plasma (ICP)-enhanced CVD and capacitively coupled plasma (CCP)-enhanced CVD, DC-PECVD, and few more CVD methods is briefly described. The structural characteristics of CNWs, using TEM/HR-TEM and Raman spectroscopy techniques and possible growth mechanism, are also discussed. Owing to their large density of nanoscale graphitic edges vertically aligned to the substrates, CNWs are potential candidates for electron field emission applications. Few examples of their field emission applications would be discussed. Further, due to the large surface area of CNWs, different electrochemical applications using CNWs such as batteries have been proposed in the literatures. Few examples of such applications would also be discussed briefly along with application of CNWs as electrode for fuel cell and solar cells.

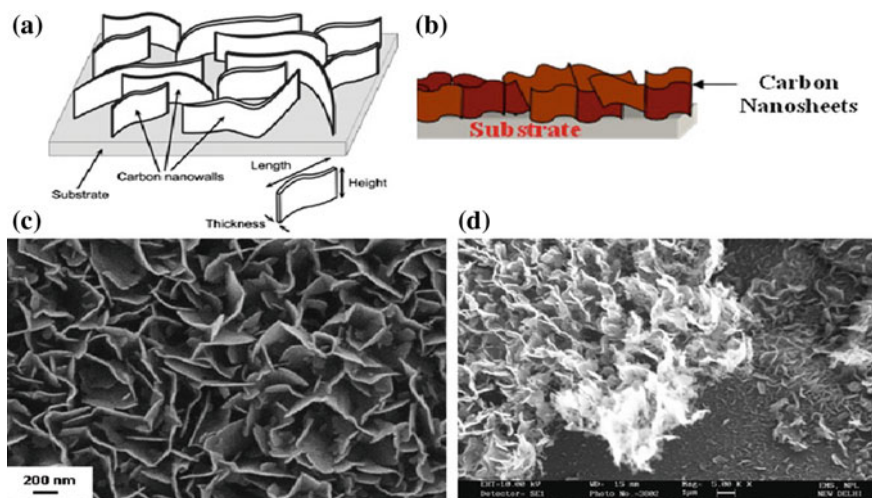


**Fig. 2.2** **a** Schematic illustration of CNWs and definition of their size. Reprinted from Ref. [53] Copyright (2005), with the permission of AIP Publishing; **b** schematic illustration of CNW in cross-sectional view, **c** SEM image of typical carbon nanowalls (prepared by microwave plasma-enhanced CVD method), **d** SEM image of CNWs in cross-sectional view



## 2.2 Growth of Carbon Nanowalls

Carbon sheets were initially observed as the by-product of CNTs by arc discharge evaporation of graphite [15, 33]. Later, Iijima et al. [34] reported production of graphite sheets or flakes coexisting with MWNTs and other form of carbon by laser ablation method. Moreover, the relative amount of sheets was very little. In this series, Ando et al. [35] proposed mass production of petal-like graphite sheets by DC-arc discharge evaporation of graphite in hydrogen gas atmosphere. However, in addition, several other forms of carbon such as MWNTs and carbon nanoparticles were also obtained. Graphite sheets were observed only in the region outside the flame of arc discharge and on the graphite wall surrounding the anode and cathode. They observed decrease in area of deposit containing petal-like sheets with increase in  $H_2$  pressure and arc current. Also, growth mechanism of such graphite sheets by the above methods was not very well understood. In addition, both the arc discharge and the laser ablation methods are high-temperature processes. The control of the process parameters to have carbon nanosheets or nanowalls of required morphology on a support material is difficult. The PECVD technique has several advantages suiting to simple and scalability to large area growth.

### 2.2.1 Main Approaches for the Growth of CNWs and Current Status

#### 2.2.1.1 Microwave Plasma-Enhanced CVD (MPECVD) Method

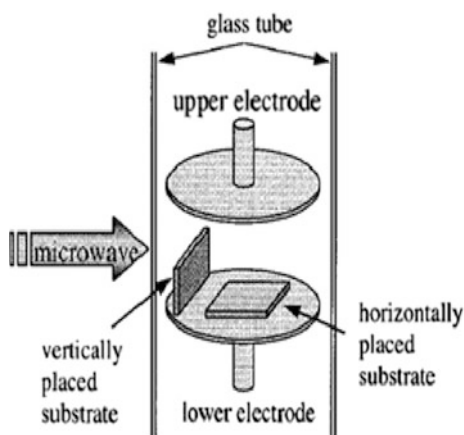
For the first time in the year 2002, Shang et al. [36] reported growth of uniformly distributed carbon nanoflakes interlaced together perpendicularly on silicon (Si) substrates by hot-filament chemical vapor deposition (HF-CVD) process using  $C_2H_2 + H_2$  gas mixture at substrate temperature (400–700 °C). They suggested that asymmetric non-Maxwellian distribution of carbon clusters and asymmetric distribution of dangling bonds of carbon atom might have favored the formation of 2-D carbon nanosheets. The same year (2002) Wu et al. [23] reported growth of 2-D CNWs standing vertically on catalyzed (NiFe) substrates (Si,  $SiO_2/Si$  and sapphire) by MPECVD under additional DC biasing during the growth of CNTs. It was the very first report on the growth of 2-D CNWs vertically standing on the substrates by a PECVD method. They used a MPECVD system, equipped with a 500-W microwave (MW) source and a traverse rectangular cavity to couple the MW to a quartz tube for generating the plasma. Two parallel-plate electrodes were placed (2 cm away from each other) inside the tube and in the longitudinal direction of the tube for applying a DC bias to promote the aligned growth of the both nanotubes and nanowalls. Schematic of the MPECVD system used by Wu et al. [23] for CNW growth is shown in Fig. 2.3. They used mixtures of  $CH_4$  and  $H_2$  gases with typical flow rates of 10 and 40 sccm, respectively. The substrate was preheated to  $\sim 650$ –

700 °C (which was basically limited by the MW power) in H<sub>2</sub> plasma without any substrate biasing. Thereafter, the CH<sub>4</sub> was introduced to the quartz tube for the growth of nanotubes. The discharge pressure was kept at 1 Torr during both pre-heating and the growth process. During the growth process, a DC bias of –185 V was applied to the substrate. It is interesting to mention that these experiments were designed to grow CNTs for scanning probe applications and therefore various types of substrates (Si, stainless steel, Cu, GaAs, and sapphire) coated with different types of catalysts (NiFe, CoFe, FeMn, FeMn, and CoCrPt) film were tried for the optimization of the CNTs growth process. Typically thicknesses of the catalysts used were from 20 to 100 nm and were deposited using sputtering system under a base pressure of  $3 \times 10^{-9}$  Torr. They found CNTs growth where the substrates were electrically connected to the biased support electrode. However, growth of CNWs without CNTs was observed when substrates were electrically cutoff or isolated from the biased supporting electrode. They accounted this due to the development of strong traverse (lateral) electric field on the sample surface due to charging of the catalyst islands (without any electrical connection between catalyst and supporting biased electrode). Typical SEM images of CNWs and HR-TEM images of CNTs obtained by Wu et al. [23, 32] are shown in Fig. 2.4.

### 2.2.1.2 Effect of Microwave Power (Density and Dimensions)

Similarly, Srivastava et al. [37] reported growth of uniformly distributed carbon nanopetals/nanowalls almost normal to the substrate on Ni- and Fe-coated Si as well as on bare Si substrates by MPECVD technique (schematic illustration of experimental setup is shown in Fig. 2.5) without any additional substrate biasing and at relatively low temperature (350–650 °C). They used mixture of argon (Ar) and methane (CH<sub>4</sub>) (9:1) as precursor gas during growth of 2-D CNWs. The Si substrates coated with Ni or Fe films (~20 nm thick deposited by thermal evaporation technique) were used for the deposition of CNW films. In this approach, the

**Fig. 2.3** Schematic of the MPECVD system used by Wu et al. [67] for CNW growth. Reprinted with permission from Ref. [67], Copyright (2002) American Chemical Society



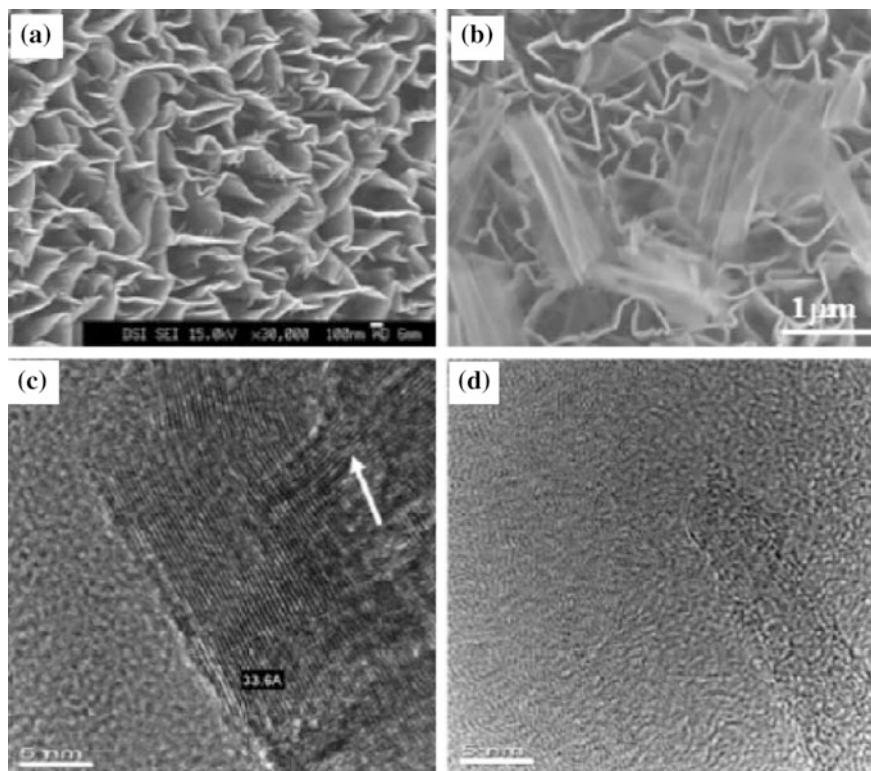


**Fig. 2.4** SEM images (a, b) and HR-TEM (c, d) images of carbon nanowalls/scale bars: **a** 100 nm, **b** 1  $\mu\text{m}$ , and **c** and **d** 5 nm. **a** was taken at a tilt angle of 25°. Reproduced (‘adapted’) from Ref. [32] with permission of The Royal Society of Chemistry

Ni-, Fe-coated, or bare Si substrates were pretreated in  $\text{H}_2$  plasma for 10 min before introducing the precursor gas ( $\text{Ar} + \text{CH}_4::9:1$ ). The process chamber pressure was maintained at 5 Torr during both preheating and the growth processes. It is to be noted that no additional heater was needed for substrate heating in this setup. The substrate heating occurred automatically by microwave induction and plasma species collisions. They investigated the effect of input MW power from 300 to 450 W on the growth and microstructures of the CNWs. The corresponding substrate temperature ( $T_s$ ) was found to vary in the range of 350–550  $^\circ\text{C}$ .

Typical SEM images of CNWs deposited under MW power of 300, 350, 400, and 450 W, respectively, are shown in Fig. 2.6a–d. These carbon films consist of high density of uniformly distributed self-sustained rose petal-like CNWs nanostructures. These petal-like CNWs have sharp edges mostly normal to the substrate. On increasing MW power and hence substrate temperature ‘ $T_s$ ’, density of petal-like CNWs increased while their size decreased (Fig. 2.6d). In addition, the petals became aligned almost normal to the substrate for higher MW power. The

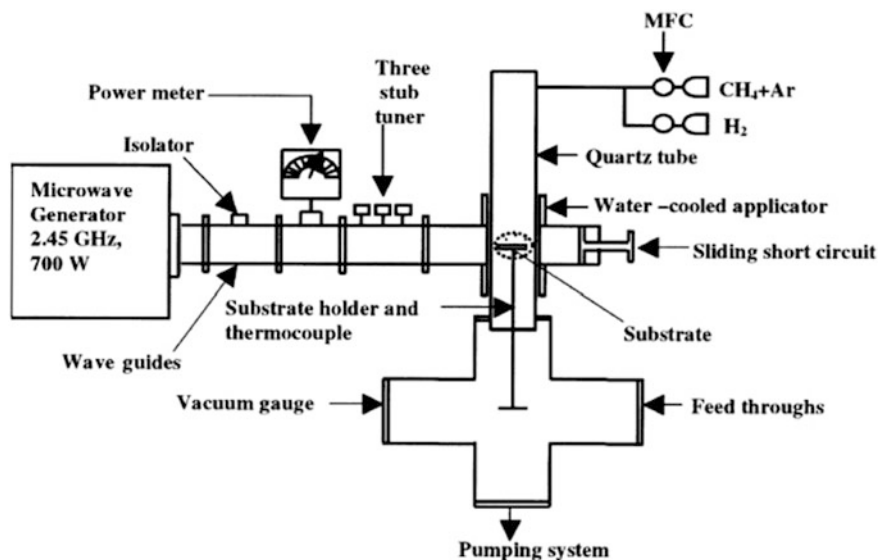


**Fig. 2.5** Schematic of the tubular MPECVD system used by Srivastava et al. [37] for CNW growth. Reprinted from Ref. [37], Copyright (2005), with permission from Elsevier

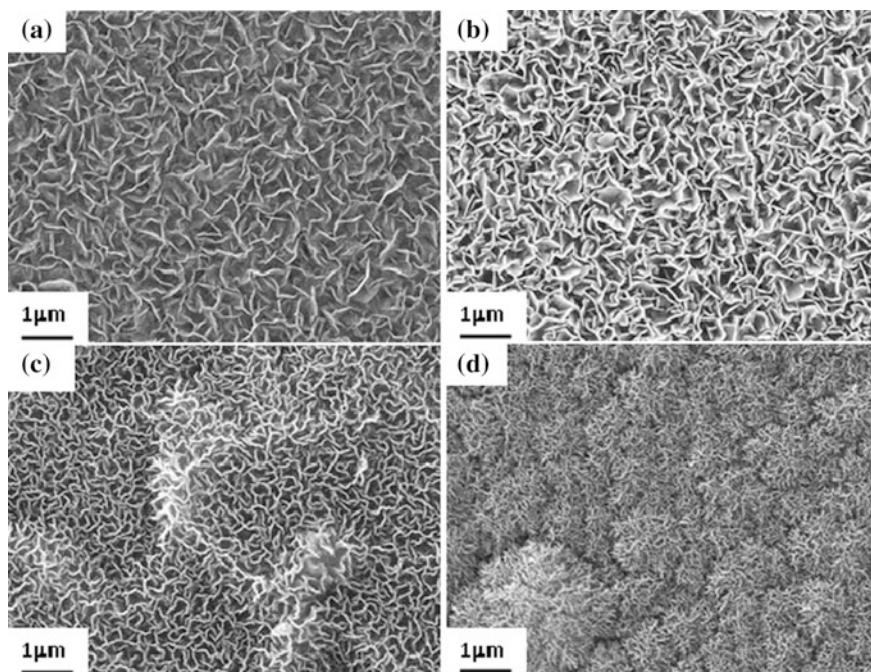
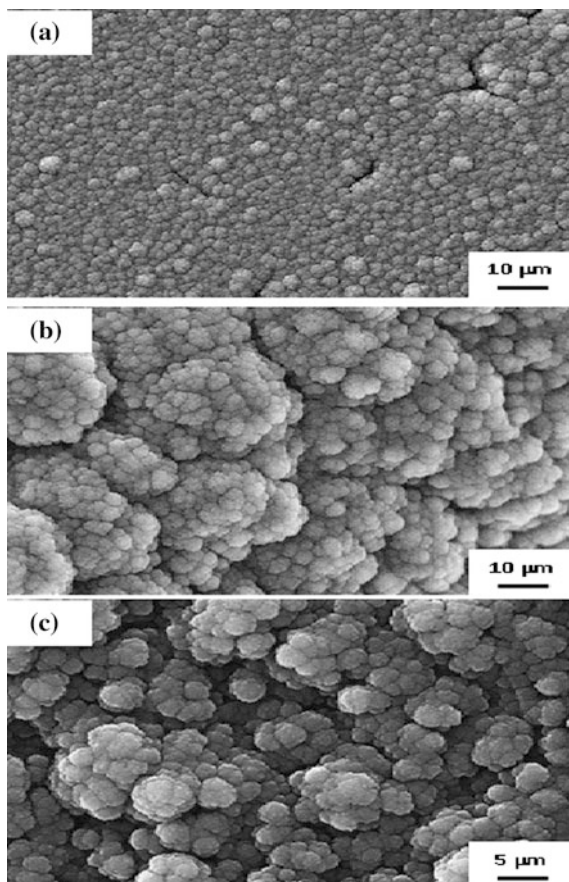


**Fig. 2.6** SEM micrographs of samples **a** 300 W, **b** 350 W, **c** 400 W, and **d** 450 W. Reprinted from Ref. [37], Copyright (2005), with permission from Elsevier

thickness of these petal-like carbon sheets for sample 300 W is estimated to be 50–80 nm which is reduced to 20–40 nm for sample 450 W. Similarly, lateral dimensions (length and width) of these nanopetals are 800–1000 nm for CNW sample deposited at 300 W and became 400–600 nm for sample deposited at 450 W.

On further increase of MW power produced no petal-like nanosheets but thick layer of amorphous carbon (a-C) with cauliflower morphology as shown in Fig. 2.7a, b for carbon films deposited at microwave power of 500 and 550 W, respectively. Similar kind of cauliflower-like structure was also observed for carbon films deposited at high discharge pressure (20 Torr) keeping MW power at 350 W and other parameters identical to that of 350 W sample (Fig. 2.7c). These results are consistent to Wu et al. [23] by MPECVD process with  $\text{CH}_4 + \text{H}_2$  mixture. However, they found CNTs/carbon nanofibers mixed with a-C for low  $\text{CH}_4/\text{H}_2$  flow rate ratio ( $\sim 1:30$ ), pure CNWs for an intermediate flow rate ratio ( $\sim 1:4$ – $1:8$ ) and a-C films for further increase of flow rate ratio at a  $T_s$  of  $\sim 650^\circ\text{C}$  and discharge

**Fig. 2.7** SEM micrograph samples deposited at **a** MW 500 W and **b** MW 550 W **c** gas pressure of 20 Torr showing cauliflower type of growth of carbon films





pressure of 1 Torr. It is interesting to note that under the similar experimental conditions as used by Wu et al. [23], Srivastava et al. [37] did not observe any CNTs growth/tubular nanostructures even in the presence of metal catalysts.

### 2.2.1.3 Effect of Catalyst and Nature of Substrates

In order to understand the role of the catalyst film on the growth of petal-like carbon nanosheets or CNWs, films were also deposited on Fe-coated Si and bare Si substrates under the same conditions as used for sample deposited at 350. In this section, samples deposited on Ni/Si, Fe/Si, and bare Si substrates are named as NP–Ni, NP–Fe, and NP–Si, respectively. Figure 2.8a–d shows the morphological features of carbon films on Fe-coated Si and bare Si substrates. The 2-D sheet morphology is also observed on these two substrates. Carbon nanosheets on Fe-coated Si are more straight and have very sharp edges normal to the substrate. Few sharp corners like whiskers are shown in Fig. 2.8a, b. On the other hand, carbon sheets on bare Si have wavy nature and surface looks uneven (Fig. 2.8c, d) compared to that on catalyzed substrates. In addition, growth rate of CNWs nanostructures was found slightly higher on Ni-coated substrates compared to Fe/Si substrate and was found the lowest on bare Si substrates.

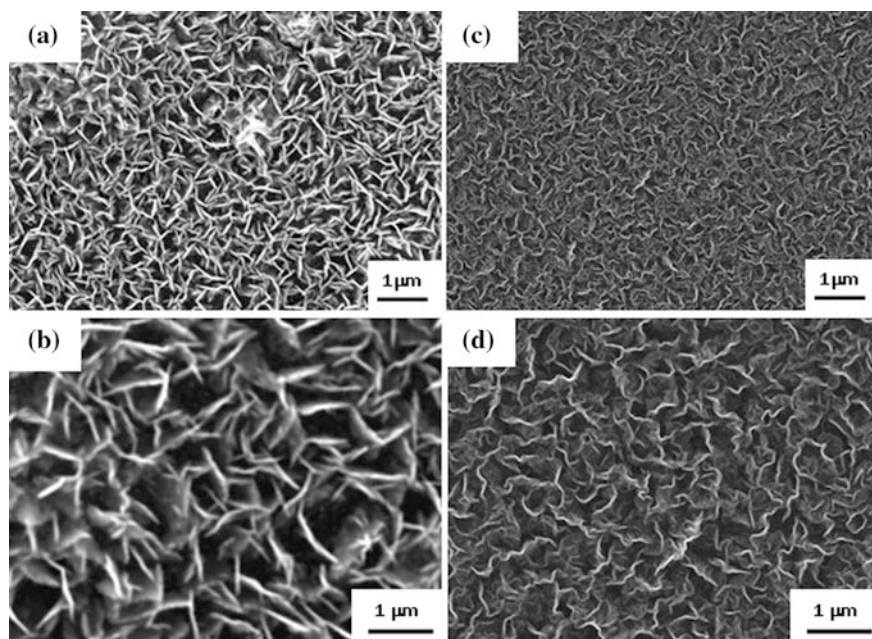
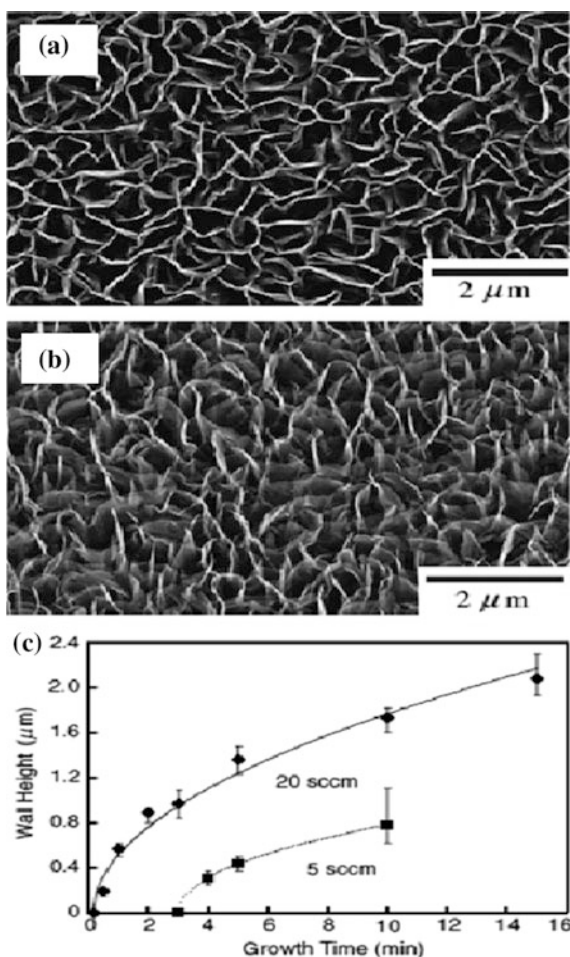


**Fig. 2.8** SEM micrographs of nanostructured carbon films showing CNWs deposited on **a** Fe/Si (sample NP–Fe) and **c** bare Si substrates (sample NP–Si). The corresponding magnified images are shown in **b** and **d**, respectively

Tanaka et al. [38] used  $\text{SiO}_2$  substrates (500 nm  $\text{SiO}_2$  on Si wafers) to investigate the growth of CNWs by using tubular MPECVD system quite similar to that used by Wu et al. [23] and Srivastava et al. [37]. The MPECVD apparatus consisted of a 2.45 GHz, 500 W of MW source, a rectangular waveguide coupled to a cylindrical glass chamber (51 mm in inner diameter and 240 mm in length). Circular parallel-plate electrodes, placed apart in the longitudinal direction of the chamber for DC biasing of the substrate. A gaseous mixture of  $\text{CH}_4$  and  $\text{H}_2$  with flow rates of  $\text{H}_2:\text{CH}_4$  of 80:20 sccm or 80:5 sccm at total gas pressure of 1.7 Torr was used for the growth of CNWs for different time. Similar to Wu et al. [23], a voltage of  $-185$  V, was applied to the substrate. Prior to CNWs growth, the substrate was exposed to hydrogen plasma for  $\sim 15$  min. Typical morphology of CNWs grown by Tanaka et al. [38] is shown in Fig. 2.9a, b. They established that the CNWs could be grown at the fine-textured structure on the  $\text{SiO}_2$  even in the absence of any catalyst. The height, thickness, and mesh size of the CNWs increased with growth time. They also could achieve very high growth rate of CNWs,  $\sim 10$   $\mu\text{m}/\text{h}$  (as shown in Fig. 2.9c), and the height of CNWs as a function of time obeys the square root law. Similarly, Wang et al. [39] used a high-power MWPCVD method to grow flat nanocarbon sheets standing vertically on Si wafers and intersecting each other at large angles. They used a MW power of 2 kW, for 3 h at substrate temperatures of  $\sim 950$   $^\circ\text{C}$ ,  $\text{CH}_4/\text{H}_2$  (15/85) gas compositions at gas pressure of 70 Torr. It is noted here that deposition rate (deposition time of 3 h) seems to be very slow in their case despite using very high substrate temperature ( $\sim 950$   $^\circ\text{C}$ ) as well as MW power and pressure in this case as compared to Wu et al. [23] and Srivastava et al. [37].

In this series, Chuang et al. [40, 41] achieved a milestone in growing three-dimensional CNWs structures. The group reported growth of CNWs by MPECVD method as freestanding structures on a metallic stage using a gas mixture of  $\text{C}_2\text{H}_2$  and  $\text{NH}_3$  without metal catalyst. They also used MPECVD setup quite similar to that of Srivastava et al. [37], but they used external DC biasing of substrates. The growth stage (as shown in Fig. 2.10a) consisted of a small cube/block of Cu or Ta mounted on the substrate holder placed in the process chamber. In this approach, the growth was metal catalysts free; however, a metal growth stage (of Cu or Ta block) was used to facilitate energy-intensive, localized plasma for the growth of CNWs. The MW plasma of  $\text{H}_2$  was ignited around the four top corners of a cubic growth stage at MW power of 500 W for 3 min, and for CNWs, growth of  $\text{H}_2$  was replaced by gas mixture of  $\text{C}_2\text{H}_2$  and  $\text{NH}_3$  maintaining the chamber pressure at 10 Torr for 10 min. Figure 2.10b shows the CNW sample attached to the Cu stage at the roots. Figure 2.10c shows a detached CNW sample against a ruler to illustrate its size. They obtained CNWs materials (both free-standing and attached to growth stage) over a wide range of growth conditions. However, formation of CNWs occurred only when a growth stage with corners were used to induce a localized, concentrated MW discharge. The normal MW plasma without metal stage was not capable of depositing such CNWs on the Si substrates. It was suggested that the formation of CNWs is energy intensive, confining the discharge to a smaller volume on the corners of the growth stage.

**Fig. 2.9** Typical SEM images of CNWs from a top view (a) and from perspective view (b), and c growth time dependence of CNWs height. Reprinted with permission from Ref. [38], Copyright 2005 The Japan Society of Applied Physics

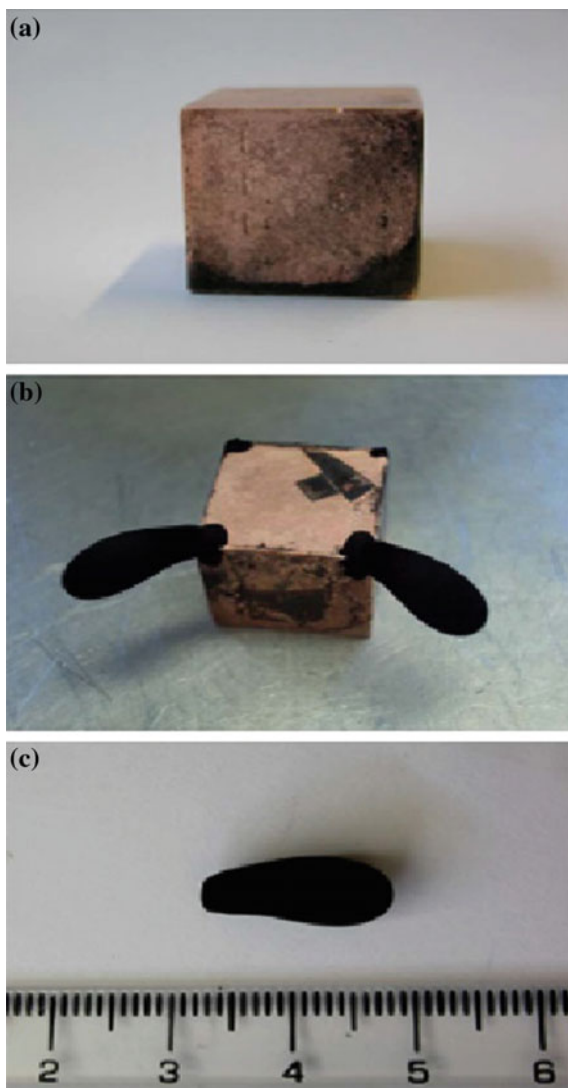


Typical SEM images of CNWs balls are shown in Fig. 2.11. It was observed that the surface-bound CNWs were more uniformly distributed and had larger wall thickness ranging 30 to 50 nm (Fig. 2.11a, b). The freestanding CNWs, on the other hand, had much smaller feature sizes, with thickness  $\sim 15$  nm, embedded in grape-like small spheres (Fig. 2.11c, d).

In summary, MPECVD has been shown a very effective PECVD technique for the growth of high-quality CNWs in a controlled manner. Since the very first report of CNWs growth by Wu et al. [23] in 2002 by MPECVD as a by-product of CNTs, several groups have successfully synthesized high-quality CNWs on different substrates by MPECVD process under various process parameters. On the basis of above experimental observations and discussions, it can be concluded that CNWs can be grown by MPECVD method in a wide range of parameters of growth temperature (as low as  $350\ ^\circ\text{C}$  to as high as  $950\ ^\circ\text{C}$ ), gas composition, microwave



**Fig. 2.10** **a** 15-mm cubic copper growth stage, **b** Nonsurface-bound carbon nanowall samples still attached to the copper growth stage at the roots, **c** A detached nonsurface-bound (freestanding) carbon nanowall sample measures to 15 mm. Reprinted from Ref. [40], Copyright (2006), with permission from Elsevier



power, and discharge pressure. In general, CNWs prepared by all the approaches have similar morphological features. It is confirmed that growth of CNWs does not require any catalyst and can be grown on both conducting and insulating substrates. This is advantageous if compared with CNTs which essentially requires transition metal catalyst by MPECVD process. Density and lateral dimensions of the CNWs can also be tailored by judiciously controlling the process parameters.

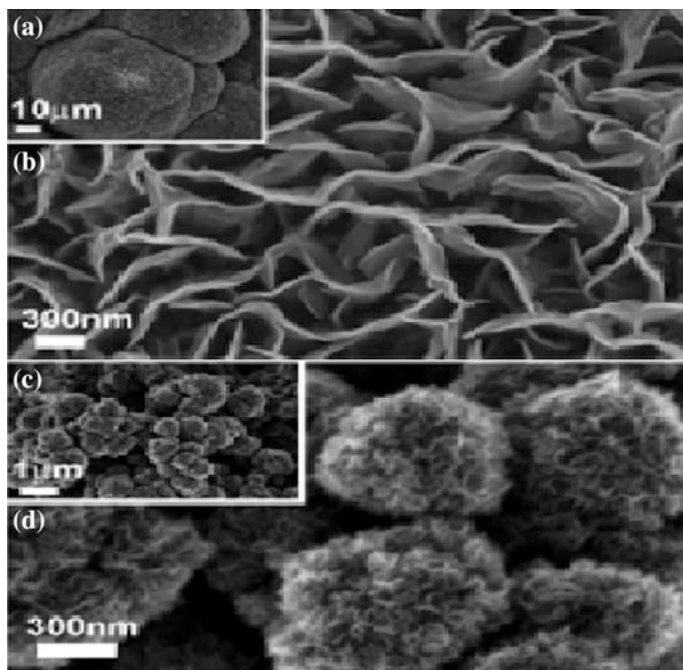


**Fig. 2.11** **a** SEM image of surface-bound carbon nanowall. Overall morphology shows spherical aggregation of nanowall structures, **b** SEM image of surface-bound carbon nanowall, showing some secondary wall-like structures, **c** SEM image of freestanding carbon nanowalls shows nanowall spheres stack to form grape-like structures, **d** SEM image of freestanding carbon nanowalls shows spheres with carbon nanowall features. Reprinted from Ref. [40], Copyright (2006), with permission from Elsevier

### 2.2.2 Growth of Carbon Nanowalls by Rf-PECVD

Radio frequency (rf)-based PECVD is another powerful technique for low temperature, large area, and controlled growth of carbon nanomaterials such as CNTs. Hiramatsu et al. [42] fabricated vertically aligned carbon nanowalls on Si, SiO<sub>2</sub>, and sapphire substrates without any catalyst by capacitively coupled plasma (CCP)-enhanced CVD in 2004 for the first time using H radical injection into the plasma. The rf-PECVD system consisted of a circular parallel-plate rf (13.56 MHz) CCP region and a remote radical source which uses an inductively coupled H<sub>2</sub> plasma (H<sub>2</sub> ICP). The circular parallel-plate electrodes were 5 cm apart. A variety of fluoro- and hydrocarbons such as C<sub>2</sub>F<sub>6</sub>, CH<sub>4</sub>, or CF<sub>4</sub> (as carbon source) into the rf-CCP region were used, and H<sub>2</sub> was fed through a 20-cm-long and 26-mm-diameter quartz tube. A five-turn rf coil connected to the rf generator of 13.56 MHz was mounted on the quartz tube. The typical process parameters for the growth of CNWs by this method were kept as follows: (a) carbon source: H<sub>2</sub> flow rates: 30:15 sccm; total gas pressure: 100 mTorr; substrate temperature: 500 °C; CCP rf power:

100 W; and ICP rf power: 400 W. In the case using  $C_2F_6/H_2$  system, aligned CNWs were grown vertically on the substrate, while CNWs grown using  $CH_4/H_2$  system were waved and thin (10 nm). However, no CNW growth was observed in the case of the deposition without H radical injection. The group has carried out pioneering work on fabrication of vertical CNWs using rf-PECVD under various gas composition and other process parameters [42–46] mostly using fluorine-based carbon sources such as  $C_2F_6$ ,  $CF_4$ ,  $CHF_3$ ,  $C_4F_8$  under similar conditions as those used for the  $C_2F_6/H_2$  system including  $CH_4/H_2$  system. They also investigated the correlation between CNWs growth and fabrication conditions under different carbon source gases. Typical morphology of the CNWs grown using the  $CH_4/H_2$ ,  $CF_4/H_2$ , and  $CHF_3/H_2$  gas systems is shown in Fig. 2.12a, b and c, respectively. The morphology of the CNWs grown using a  $CF_4/H_2$  and  $CHF_3/H_2$  system was similar to those using the  $C_2F_6/H_2$  system with marginal differences in the spacing between the walls. But CNWs could not be grown with  $C_4F_8/H_2$  system. The growth rates (wall height vs. growth period) of CNWs had almost linear relationship with the growth period for  $C_2F_6$ ,  $CH_4$ ,  $CF_4$ , or  $CHF_3$  systems as presented in Fig. 2.13. It was found to be the highest for the  $C_2F_6/H_2$  system and the lowest for the  $CF_4/H_2$  system. Therefore, the  $CF_3$  radicals were proposed to be important species responsible for the formation of CNWs in any fluorocarbon/hydrogen systems. Similarly, the  $CH_3$  radicals generated by a  $CH_4$ -CCP in the  $CH_4/H_2$  system were also considered to be important species for CNWs growth for  $CH_4/H_2$  system. Based on extensive investigations, the group concluded that H atoms play an important role in the formation of the CNWs. Injected H atoms react effectively with fluorocarbon radicals in the gas phase as well as at the surface by the reaction of F abstraction. At a substrate temperature of 500 °C, H atoms play key role in producing  $sp^2$ -bonded carbons at the surface and hence a continuous  $sp^2$  network, which eventually results in the formation of CNWs. Later, the group also measured [43] H atom density in the plasma using vacuum ultraviolet absorption spectroscopy (VUVAS), in order to confirm the role of H atoms on the growth of CNWs.

Similarly, another group [47, 48] reported the growth of freestanding and ultrathin graphitic sheets ( $\sim 1$  nm thick) using an inductively coupled rf-PECVD method on variety of substrates including metals, semiconductors, and insulators (Si,  $SiO_2$ ,  $Al_2O_3$ , Mo, Zr, Ti, Hf, Nb, W, Ta, Cu, and 304 stainless steel), without catalyst, and under various growth conditions using  $CH_4/H_2$  system. They also confirmed H incorporation into the CNWs by means of infrared and thermal desorption spectroscopies and suggested that a combination of high plasma electron density and large atomic H density of the ICP accounted for CNWs formation. Similarly, several other groups have also demonstrated growth of CNWs by using rf-based PECVD method (CCP, ICP or in any other modes) [49–51]. It is also worth mentioning that among PECVD methods, not only high-frequency sources (such as rf or MW) have been used for the growth of CNWs but other simpler PECVD techniques such as DC-PECVD [52–57] have also been used for high-quality CNWs growth. In addition, there are few examples of CNWs growth by hotwire CVD (HW-CVD) and hot-filament CVD (HF-CVD) methods (with or

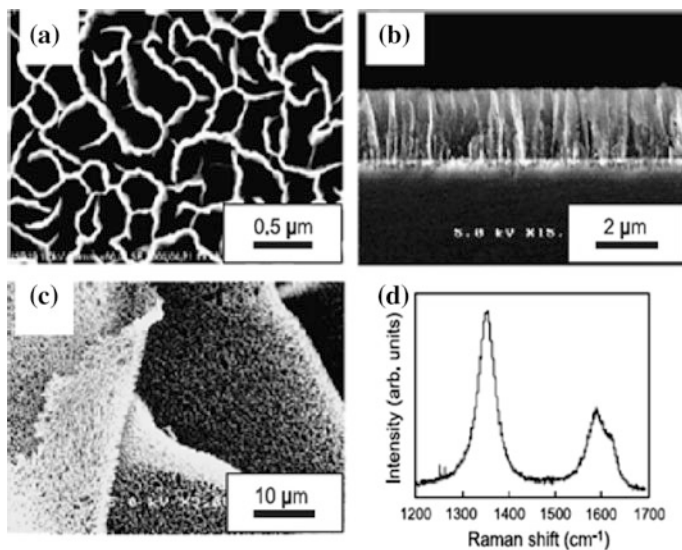
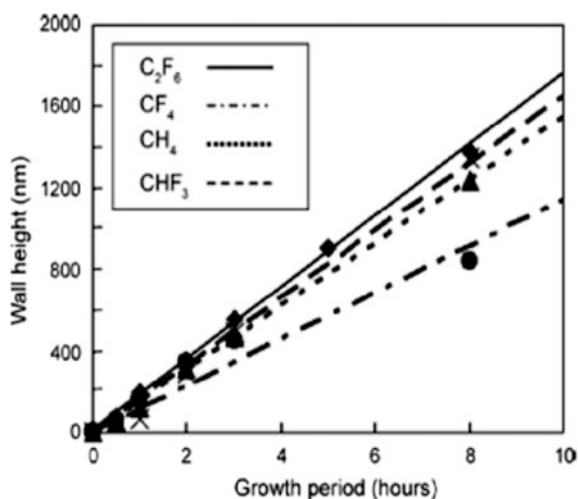


**Fig. 2.12** SEM images of the carbon nanowalls grown on Si substrate using  $C_2F_6$  rf-CCP assisted by H atom injection for 8 h; **a** top view and **b** cross-sectional view, **c** An SEM image of carbon nanowall that was scratched from a Si substrate, **d** Raman spectrum for the carbon nanowalls in (a). Reprinted from Ref. [43], Copyright (2005), with permission from Elsevier

**Fig. 2.13** Carbon nanowall height, as a function of the growth period. Growth data was obtained from the samples grown using  $C_2F_6$  (solid line),  $CF_4$  (dash-dot line),  $CH_4$  (dotted line), and  $CHF_3$  (broken line) as the carbon source gas. Reprinted from Ref. [43]. Copyright (2005), with permission from Elsevier



without DC plasma assisted) [58, 59] also. However, growth of CNWs by conventional thermal CVD is rarely reported and efforts are being made. Nevertheless, PECVD has been a proven method for CNWs growth and can be scaled up on large area as well.

## 2.3 Characterization of CNWs

The CNWs synthesized by any methods so far have mainly characterized by scanning electron microscopy (SEM), transmission electron microscopy (TEM) and high-resolution TEM (HR-TEM), and Raman spectroscopy. The SEM has been used for morphological and growth characteristics of the CNW films whereas TEM and HR-TEM and Raman spectroscopy techniques have been used very efficiently for the structural characteristics of the CNWs irrespective of the growth methods (plasma or nonplasma-based techniques).

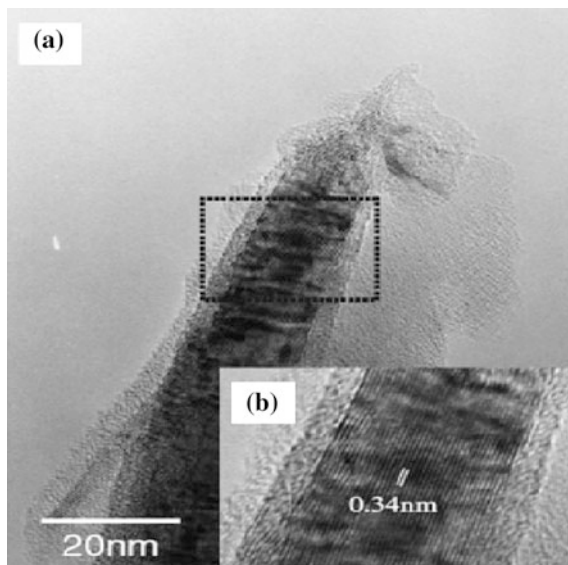
### 2.3.1 CNW Structure by HR-TEM

Figure 2.14 shows a typical HR-TEM micrograph of 2-D CNWs prepared by MPECVD method [38]. The nanowalls, as shown in Fig. 2.14a, are made up of many individual graphite/graphene walls. The HR-TEM image reveals the crystallinity as well as interplanar spacing of the walls in each CNW. The interplanar spacing is  $\sim 0.34$  nm confirming that the CNWs are made of few to several layers of graphene. Also, since mostly, growth of CNWs is carried out by PECVD route which is a relatively low-temperature growth process, it results in the presence of defects in the CNWs. Such defects can be observed from the HR-TEM images. The HR-TEM image of CNWs shows regions of highly graphitized and disordered amorphous phases (Fig. 2.14b).

### 2.3.2 CNWs Structure by Raman Spectroscopy

The Raman spectroscopy is a very powerful, nondestructive technique for the structural characterization of different carbon nanomaterials. This technique is also used extensively for the quality of the CNWs irrespective of growth technique. For example, first-order Raman spectra of CNWs samples grown at input MW powers of 300, 350, 400, and 450 W by MPECVD method are shown in Fig. 2.15 [37]. In these spectra, two characteristic signals are observed. Strong peaks at  $\sim 1350$  and  $1580\text{ cm}^{-1}$  are typical D and G bands of microcrystalline graphite [60]. The strong D peak indicates that CNWs consists of a more nanocrystalline structure and defects such as distortion, vacancies, and strain in graphitic networks, which are typical features in CNWs. An additional peak at  $\sim 1620\text{ cm}^{-1}$  called as  $D'$  is also observed as shoulder to G peak. The Raman spectra of CNWs are similar to those of the MWCNTs [61]. The CNWs deposited at different MW powers essentially have both D and G bands. However, the intensity ratio of the D to G bands [ $R = I(D)/I(G)$ ], full width at half maximum (FWHM) of the D and G bands as well as the intensity of the  $D'$  band increased considerably with higher input MW power in

**Fig. 2.14** Typical **a** high-resolution TEM image of CNW, **b** enlarged TEM image for the rectangular section in **(a)**. Reprinted with permission from Ref. [38], Copyright 2005 The Japan Society of Applied Physics



MPECVD process. Typical variation of intensity ratio of  $D$  and  $G$  bands [ $I(D)/I(G)$ ] and FWHM of  $D$  band versus MW power is shown in Fig. 2.16 [37] and is also in accordance with the observation by Tuinstra and Koenig [62]. The shift in  $G$  peak from  $1581$  to  $\sim 1600\text{ cm}^{-1}$  [63, 64] and increase in  $I(D)/I(G)$  ratio correspond to transformation from graphite to nanocrystalline graphite phase. This shift of  $G$  peak to higher wave number is also due to evolution of  $D'$  band, at  $\sim 1620\text{ cm}^{-1}$ . For smaller crystallites, the  $D'$  peak merges into the  $G$  peak and a net of the intensity of  $G$  feature is observed as a result of overlapping of the intensity of  $G + D'$  feature [63]. The position of the maximum in the  $G + D'$  feature is also observed to shift to higher wave number with higher MW power. This again indicates that the CNWs grown at higher MW power consist of higher degree of disorders and relatively smaller size or nanographitic crystallites. In general, the CNWs grown by any PECVD technique have these Raman characteristic peaks,  $D$ ,  $G$ , and  $D'$  peaks [37, 38, 40, 41, 53, 54, 65, 66] and are established that CNWs consist of graphitic nanostructures/small crystallites with high degree of defects.

## 2.4 Growth Mechanisms of CNWs

The above experimental investigations suggest that 2-D CNWs can be fabricated by variety of PECVD techniques irrespective of the growth process and conditions. It means there has to be a common mechanism of nucleation and growth of these 2-D carbon nanostructures, which is not fully understood. It has been proposed by Wu and coworkers that the electrical field is the most important factor in a MPECVD

**Fig. 2.15** Raman spectra of the petal-like nanostructured carbon films deposited at different microwave power. Reprinted from Ref. [37], Copyright (2005), with permission from Elsevier

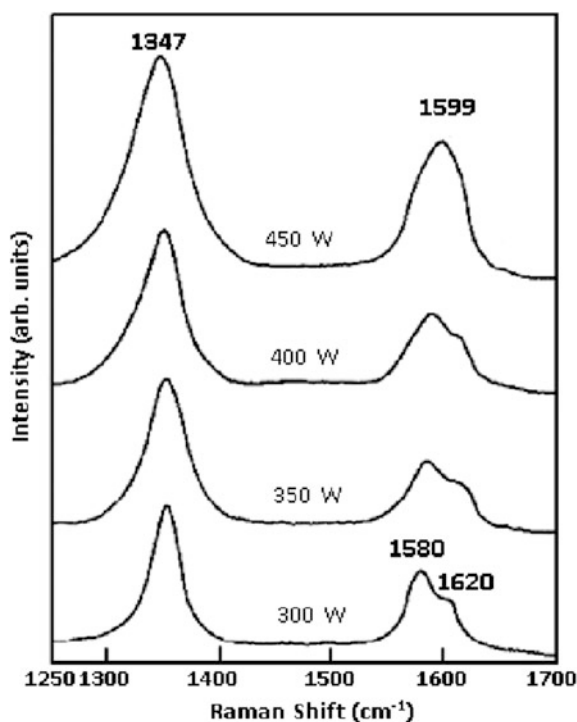
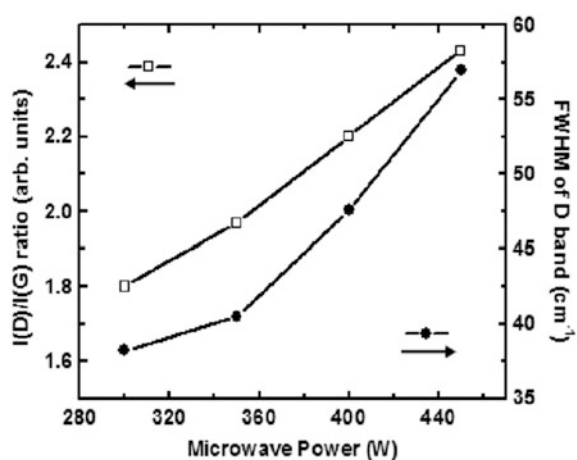


**Fig. 2.16** Variation of  $I(D)/I(G)$  ratio and FWHM of D band of carbon films deposited at different microwave power. Reprinted from Ref. [37]. Copyright (2005), with permission from Elsevier



process [23, 67]. However, the same may be valid in case of the other plasma assisted CVD processes such as rf-PECVD, DC-PECVD. The source of the electrical field in a MPECVD setup is first due to applied DC bias. The nonuniform charging up of the substrate in the plasma which can be altered by the existence of



metallic particles and other types of sharp features such as metal slabs/block as used by Chuang et al. [40, 41] also plays critical role. It has been found that in metallic particles presence which act both as a catalyst as well as field modulator, both CNTs and CNWs can be formed depending on the strength of the lateral electrical field and other growth parameters such as the gas flow rates, temperature, and pressure [23]. However, in the absence of catalytic metal particles or on bare substrates, it is more likely that only CNWs will be formed. To understand the mechanism of CNWs formation, Srivastava et al. [37] investigated growth of CNWs with varying growth time keeping all other parameters constant. Figure 2.17 shows the representative SEM images of the CNWs at different growth stages on the Ni (20 nm)/Si as well as on bare Si substrates. During the preheating stage, the Ni thin film changed to isolated nanoparticles. The image in Fig. 2.17a shows the initial stage of the growth process wherein formation of large size clusters of Ni as a result of H<sub>2</sub> plasma pretreatment are observed. The time evolution of surface morphology suggests that in the initial stage of growth of carbon films, tiny sheets are formed (Fig. 2.17a, b) which grow in size (both lateral and vertical directions) as the deposition time is increased (Fig. 2.17c–e). This resulted in carbon nanosheets as large as ~600–800 nm as shown in Fig. 2.17f. The observation is consistent with the observations by Wu and co workers using Au, and other transition (Ni, Fe, etc.) metals as catalyst which implies that the existence of a strong lateral field is the key to growing CNWs. Wu and Yang have done detailed investigation on the role of electrical field in the growth of CNWs [67]. An important observation of Srivastava et al. [37]’s investigation is that without any external biasing the petal-like CNWs were obtained almost normal to the substrate surface. This suggests that the growth of CNWs could be influenced by the self-bias potential established on the immersed substrate surface in the high-frequency plasma, the field lines of which are invariably terminated normal to the surface [68, 69]. The electrostatic force would help the carbon sheets to align with the field direction which is perpendicular to the substrate surface and an energetically favorable orientation. Demonstration of growth of three-dimensional macroscopic freestanding CNWs structure purely catalyst-free and unconstrained by substrate surfaces [40, 41] is another example of electric field-driven growth of CNWs. Other detailed growth mechanisms proposed by different groups also emphasize the important role of electric field in the controlled growth of CNWs [70, 71].

With increase in MW power in a tubular MPECVD setup and hence the higher substrate temperature, CNWs are found to grow, with sharp edges further aligned normal to the substrate surface. It is expected that increase in MW power causes higher degree of ionization of the gas, increasing the density of relatively high-energy plasma species and hence higher magnitude of the self-bias of the substrate surface. Increased nucleation of graphitic clusters is expected to occur, and this leads to the formation of CNWs of relatively smaller size and higher density at increased MW power (as shown in Fig. 2.6d). Further increase of input MW power leads to deposition of disordered amorphous carbon structures. Increase of discharge pressure also leads to higher density of plasma species and hence higher substrate temperature resulting in disordered amorphous cauliflower



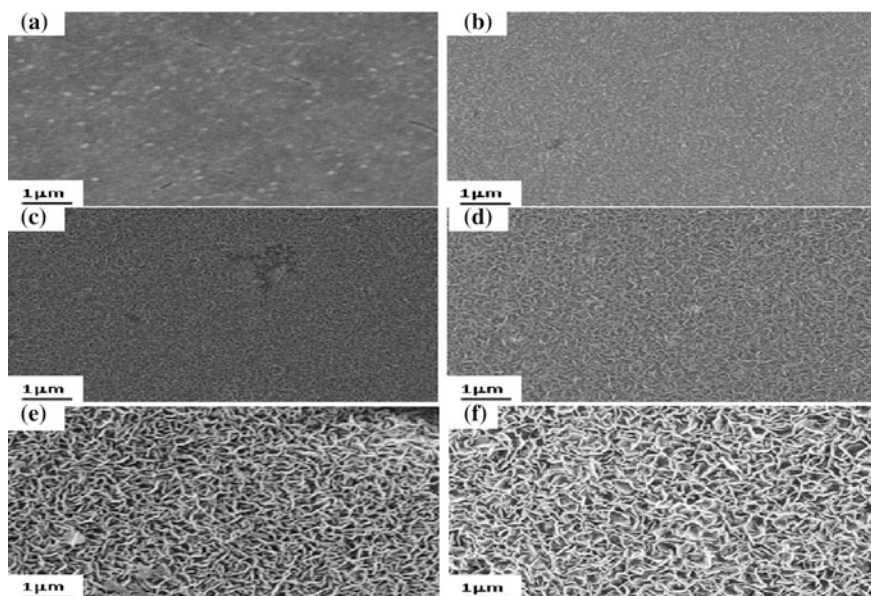


**Fig. 2.17** SEM micrograph of **a**  $H_2$ -plasma-treated Ni film and carbon films deposited at microwave power of 350 W for **b** 2, **c** 5, **d** 10, **e** 20, and **f** 30 min. Reprinted from Ref. [37]. Copyright (2005), with permission from Elsevier

structures. These observations also suggest that the CNWs can be grown only for a moderate rate of carbon supply at a given substrate temperature in the tubular MPECVD setup. This is confirmed by low-magnification SEM image of sample grown at 550 W of MW power. The image is recorded near the boundary of the highest intensity plasma (HIP) ball (Fig. 2.18). The magnified images were taken from different portions of the same substrate (as shown in Fig. 2.18) which was placed on the substrate holder in such a way that the growth rate would vary from one side to the other due to the offset from the optimum position. The figure shows relative decrease of growth rate of film with increasing distance from the optimum position (HIP zone). The corresponding morphologies of the sample are shown by magnified images as presented in Fig. 2.18. It is clear that CNWs are formed only in the edge region of the HIP zone where plasma density and hence substrate temperature is supposed to be lower relative to that within HIP zone. On increasing the distance from the HIP zone, density of the sheets decreases and is the least at the outermost region of the plasma. The dimensions of the CNWs first increase and then decrease toward outer zone. The decrease of the dimensions at the outer most regions could be due to very slow growth rate. The observation further confirms the important role of input MW power and hence the self-biasing/electric field in the growth of CNWs in PECVD process.

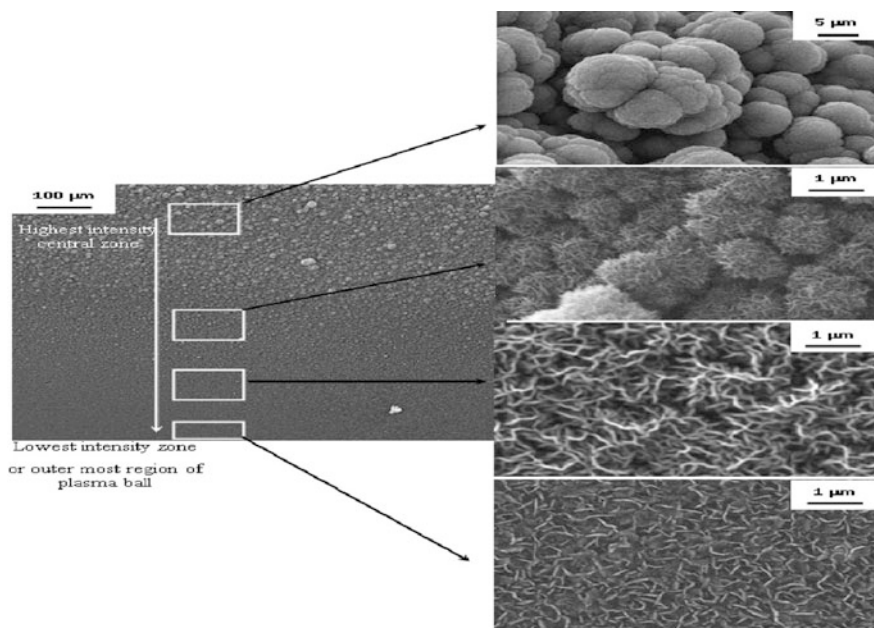


**Fig. 2.18** Low-magnified SEM micrograph of a sample deposited at 550 W of MW power near the boundary of the highest intensity plasma (HIP zone) of tubular MPECVD showing variation of growth rate and morphology with distance from the HIP central zone and the corresponding magnified images

## 2.5 Field Emission Properties of Carbon Nanowalls

### 2.5.1 Field Emission

Field emission (FE) is the ejection of electrons from a solid surface under the effect of high electric field of the order of  $10^9$  V/m. When such a field is applied to a solid surface with a negative bias, electrons inside the solid are emitted into vacuum by quantum mechanical tunneling effect [72]. Such high field can be obtained on a sharp tip of a very thin needle where electric field lines concentrate. The schematic of quantum mechanical tunneling of electrons from a solid surface under the applied electric field is shown in Fig. 2.19 [73]. Microwave generators, X-rays, e-beam evaporators, mass spectrometers, display devices, etc., rely on thermionic electron emitters operating in a temperature range of 1000–2000 °C. Due to the high operating temperatures, miniaturization of thermionic emitters is strongly limited. Field electron emitters operating at room temperature, on the other hand, have great potential for miniaturization and hence portability of a device. This opens up several new applications such as flat panel displays, data storage devices. However, the development of FE electron sources remained hampered for about half a century due to the fact that tip-like field-enhancing structures needed to create

local high electric fields for FE to take place were under investigation. Critical life time and high operating voltages are additional intriguing factors [74]. An ideal electron source, in a micrometer sized device, has to meet several important requirements: For example, it should have a high mechanical strength and melting point, good electrical and thermal conductivity, low work function, stable chemical properties, and be inexpensive and easy to process [75]. A variety of field emitting thin films such as microcrystalline diamond films, nanodiamond films, diamond like carbon films [76] have been proposed as an alternative to the conventional tip arrays of emitters for reduced fabrication cost and improved robustness [77]. In this series of carbon materials, a lot of attentions have been paid to CNT (both SWNTs and MWNTs)-based field emitters. The potential of CNTs for FE was first reported in 1995. FE from an isolated single MWNT was first reported by Rinzler et al. [78] and that from a MWNT film was reported by de Heer et al. [79]. Since then, a number of experimental studies on FE aspects of both MWNTs [80–97] and SWNTs [98–101] have been carried out. FE from CNTs has shown to be one of the most promising properties as far as its practical application is concerned. This is because CNTs present many advantages over conventional emitters due to their unique structure and properties such as (i) high chemical stability (resistance to oxidation or other chemical species) and high mechanical strength (Young's modulus  $\sim 1$  TPa), (ii) high melting point ( $\sim 3550$  °C) and reasonable conductivity (resistivity  $\sim 10^{-7}$   $\Omega\text{m}$ ), (iii) high aspect ratios ( $>1000$ ) with very small tip radius to greatly enhance the local electric field, and (iv) large-scale production at low cost, have longer life time, and are capable of low operating voltages [75].

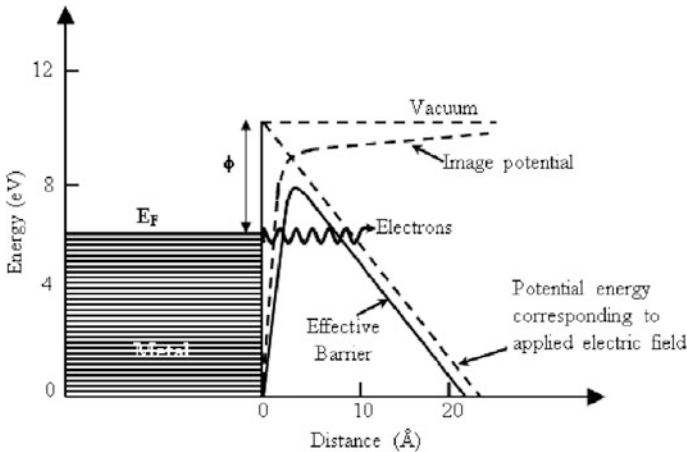


**Fig. 2.19** Potential energy diagram illustrating the quantum mechanical tunneling of electrons under an external electric field. Reprinted from Ref. [73]

### ***2.5.2 Field Emission Properties of Carbon Nanowalls***

The unique morphology and geometrical shape of carbon nanowalls (as described in the earlier sections) can bring about many fascinating properties such as field emission. Moreover, the intrinsic disorders and defects of CNWs are likely to alter these properties and are ideal candidates for electron transport studies. Previously, field emissions have been studied. In the following section, brief description of a basic experimental setup for field emission measurements, basics of field emission process and related parameters, and finally the state of the art of the FE properties of CNWs are being presented.

### ***2.5.3 Field Emission Measurement Setup***

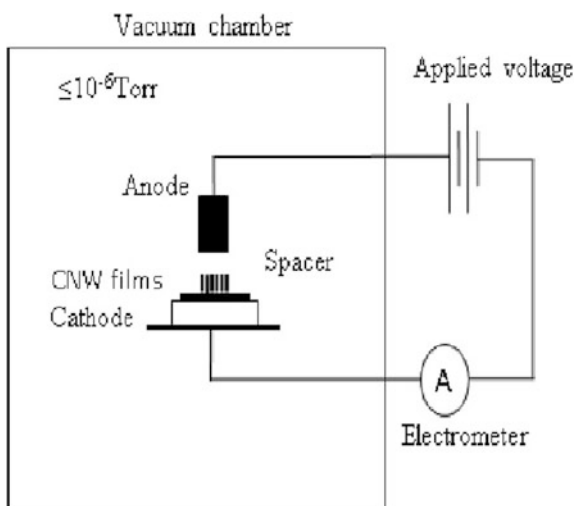
The FE measurements of nanostructured carbon films are carried out in a high-vacuum chamber using a simple diode configuration. The schematic diagram of FE measurement setup is shown in Fig. 2.20. It consists of a high-vacuum chamber the base of which is connected to a 6-inch-diameter diffusion pump (model 160/700 M, Edwards, UK) backed by a mechanical rotary pump (Edwards). Pressure in the chamber was monitored by a Pirani/Penning gauge (model PRL10 K, Edwards, UK). The electrodes of the assembly are made of circular Cu plates or any other vacuum compatible and conducting metal. Lower electrode was made as cathode (CNW films), and the sample was fixed to it with the help of silver paste. The electrode holding the sample was connected to a high-voltage power supply through an electrometer in series. Sometimes, a high resistance (of 1 M $\Omega$ ) is also connected in series with the electrometer to limit the current in maximum range of the electrometer. The upper electrode which was movable in the Z-direction was connected to the positive terminal of the supply. It also had graduated circular plate with the help of which the gap between the electrodes could be adjusted. The upper electrode assembly could be removed for mounting the sample. The distance ( $d$ ) between the top emitting surface of the film and anode was determined by first lowering the anode to the sample until electrical contact was observed then lifting the plate to a certain value with the help of the scale made on the anode. The value of  $d$  was adjusted between 300 and 500  $\mu\text{m}$  as per the nature of the sample of CNWs. Several groups also use separation layer of Teflon sheet/tape of different thickness between cathode (CNWs samples and the anode). The FE measurement is generally performed in high vacuum (at a pressure of  $\leq 2.0 \times 10^{-6}$  Torr) at room temperature. The variable positive voltage is applied to the anode in steps and the emission current is measured by the suitable electrometer. It is to be noted that conditioning of each sample is crucial and essential before the final measurements of emission current by applying a high voltage to remove any kind of impurity such as adatoms or adsorbates on the surface of the CNWs. The macroscopic electric field ( $E$ ) applied between the electrode is estimated by dividing the applied voltage

( $V$ ) by the sample-anode separation ( $d$ ) ( $E = V/d$ ). The emission current density ( $J$ ) can be calculated by dividing measured current with the area of the CNWs sample exposed to the anode.

The field emission characteristics is usually analyzed by Fowler–Nordheim (F–N) theory [72], according to which the emission current density ( $J$ ) from a metal tip/surface is dependent on the local electric field ( $E_{\text{loc}}$ ) and chemical state of the (i.e., work function,  $\phi$ ) of the emitter surface as  $J \propto (E_{\text{loc}}^2/\phi) \exp(-B\phi^{3/2}/E_{\text{loc}})$ , where  $B = 6.83 \times 10^9 \text{ V eV}^{-3/2} \text{ m}^{-1}$ . The schematic of electron emission methodology from an emitter under the applied electric field and relation between the  $E_{\text{loc}}$  and the  $E$  and corresponding F–N formula are shown in Fig. 2.21a. In case of CNW-based cathode films, electron emission occurs from the multiple emitters and an average or integrated current is measured. There is lot of variation of local field on emitters tip in CNW films due to variation in local morphology/nanoscale emitter geometries. Also, the work function of each emitter may not be the same due to which the exact analysis of FE characteristics of CNW films is a difficult task. Nevertheless, F–N theory is the most suitable one and has been used for interpretation of emission properties of not only CNWs but also various other carbon nanomaterials including SWNTs and MWNTs. In this model, there are two key parameters in F–N formula,  $\phi$  and  $E_{\text{loc}}$ , where  $E_{\text{loc}}$  is related to  $E$  by geometrical enhancement factor ( $\beta$ ) as  $E_{\text{loc}} = \beta E$ . The value of  $\beta$  can be determined experimentally from the slope of F–N plot between  $\ln(I/V^2)$  versus  $1/V$ , provided  $\phi$  is known. The slope of F–N plot is given by,

$$\text{Slope} = -\frac{B\phi^{3/2}d}{\beta}. \quad (1)$$

**Fig. 2.20** Schematic of field emission measurement setup



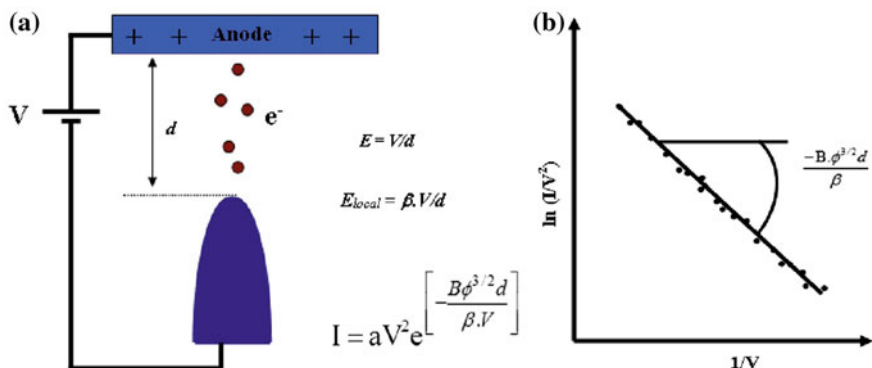


**Fig. 2.21** **a** Principle of FE from a curved surface and the F–N formula. **b** An ideal F–N plot for FE showing *straight line* with negative slope

An ideal F–N plot for electron field emission characteristics is shown in Fig. 2.21b. Typically, field emission quality of emitter is quantified with respect to two parameters called as turn-on field ( $E_{to}$ ) and threshold field ( $E_{th}$ ). Typically,  $E_{to}$  is the field (in  $V/\mu m$ ) required for emission current density of  $10 \mu A/cm^2$  and  $E_{th}$  is the field required to achieve  $1 mA/cm^2$  emission current density from the emitter. Third parameter is related to the stability and uniformity, reproducibility, and lifetime of emission current (at  $E_{to}$  and  $E_{th}$ ) for as long as possible duration.

### 2.5.3.1 Field Emission Characteristics of CNW-Based Carbon Films

Since CNW films contain a high density of uniformly distributed vertical carbon nanosheets or nanowalls, with sharp graphitic edges normal to the substrate, the CNWs are supposed to exhibit high geometrical enhancement factor for the electric field and hence a very good electron emission. Herein, few examples of FE properties of CNW films prepared by MPECVD process are illustrated. Also, the effect of various process parameters on the FE properties of such CNW-based emitters is briefly presented.

### 2.5.3.2 Effect of Catalyst–Substrate Interaction on the Field Emission

Field emission measurements of CNW films deposited on Ni/Si, Fe/Si, and bare Si (samples NP–Ni, NP–Fe, and NP–Si, respectively) by MPECVD method at MW power of 350 W under  $CH_4/Ar$  gas composition for deposition time of 30 min and discharge pressure of 5 Torr (please see morphology of such CNW films in Fig. 2.8) are shown in Fig. 2.22. It is shown that catalytically grown samples exhibited superior emission characteristics to that on bare Si-based CNW films. The emission current density ( $J$ ) versus the macroscopic electric field ( $E$ ) plot of these

**Fig. 2.22** **a** Emission current density versus macroscopic field of nanostructured carbon films grown on Ni/Si, Fe/Si, and bare Si **b** corresponding F–N plots

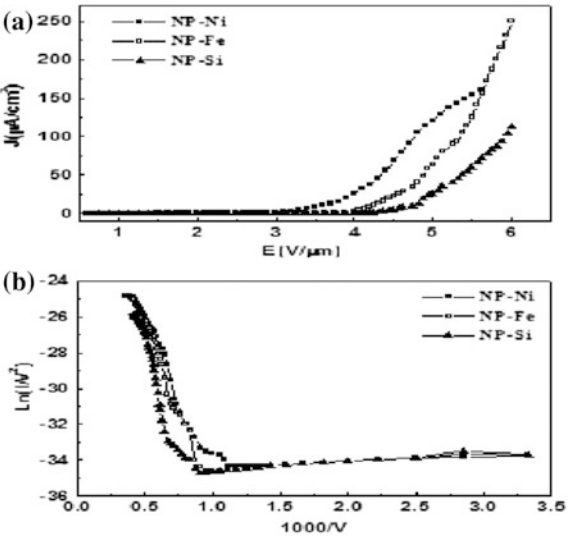


**Table 2.2** Comparison of FE parameters ( $E_{to}$  and  $E_{th}$ ) of CNW films grown on Ni/Si, Fe/Si, and bare Si substrates

Sample	Turn-on field ( $E_{to}$ ) (V/μm)	Field enhancement factor ( $\beta$ )
NP–Ni	3.60	2428
NP–Fe	4.25	2110
NP–Si	4.75	1926

samples is shown in Fig. 2.22a and the corresponding F–N plot in Fig. 2.22b. The corresponding  $E_{to}$  and  $E_{th}$  values are listed in Table 2.2. The CNW films on Ni-coated Si substrate were found to have the lowest  $E_{to}$  while those on bare Si had the highest among these films. It indicates that the interface resistance between the film and the substrate may have significant role in the FE process in addition to the density and morphological features (density of sharp edges in the CNWs). It is known that formation of  $NiSi_x$  occurs at lower temperature ( $>300\text{ }^{\circ}\text{C}$ ) [96] while reaction between Fe and Si substrate is a high-temperature process. Therefore,  $FeSi_x$  formation is unlikely to occur at temperatures ( $\sim 400\text{ }^{\circ}\text{C}$ , the substrate temperature corresponding to 350 W of MW power) [102]. Formation of  $NiSi_x$  may lower the interface resistance and hence facilitate the transport of electrons across the CNWs/ $NiSi_x$  interface. This could be the possible reason for the good FE characteristics of CNW films on Ni/Si substrates compared to that on Fe/Si or bare Si substrates despite almost identical surface morphological features.



**Fig. 2.23** a Emission current density versus macroscopic field of petal-like nanostructured carbon films with varying microwave power **b** corresponding F–N plots. Reprinted from Ref. [37], Copyright (2005), with permission from Elsevier

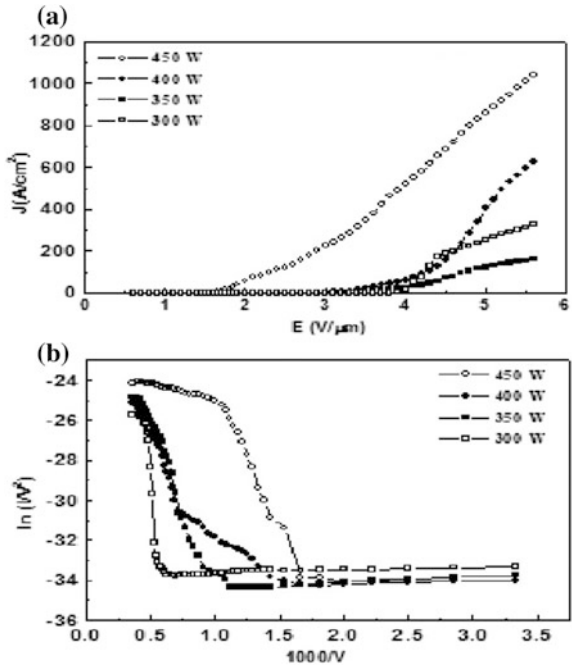


**Table 2.3** Comparison of FE parameters ( $E_{to}$  and  $E_{th}$ ) of petal-like CNW films

Sample	Turn-on field ( $E_{to}$ ) (V/ $\mu$ m)	Threshold field ( $E_{th}$ ) (V/ $\mu$ m)
NP300	4.00	–
NP350	3.60	–
NP400	3.35	–
NP450	1.75	~ 5.60

2.5.3.3 Effect of Microwave Power (Density and Dimensions of CNWs)

Srivastava et al. [37] investigated the effect of microwave power on the growth and field emission characteristics of CNW films by MPECVD method. The  $J$  versus  $E$  plots of CNW-based films prepared for microwave power of 300, 350, 400, and 450 (named as NP300, NP350, NP400, and NP450, respectively) by MPECVD are given in Fig. 2.23a. Among these, the best emission characteristics were observed in 450 W sample. The observed  $E_{to}$  and  $E_{th}$  values for these samples are given in Table 2.3. The observed  $E_{to}$  values are much lower than the values (17–35 V/ $\mu$ m) reported by Shang et al. [36] for such films by HF-CVD process. The  $E_{to}$  values decreased for samples deposited at higher MW power and the lowest  $E_{to}$  value was observed for sample 450 W. The increased density, smaller size, and improved alignment of CNWs are possibly responsible for the decreased  $E_{to}$  values for samples deposited at higher MW power. The corresponding F–N plots for the four



CNWs samples (as shown in Fig. 2.23b) have straight line with negative slopes in the high field region indicating that the emission process from the CNW films is primarily governed by the F–N model.

Similarly, other groups have also shown excellent FE properties from CNW films [32, 39, 58, 103–115] with turn-on fields as low as 1 V/ $\mu\text{m}$  or lower, which are comparable to the turn-on fields for CNTs or graphene films [80–101].

#### 2.5.3.4 Effect of Temperature on the FE Properties of CNWs

Wu et al. [32] also have reported FE properties of CNWs prepared by MPECVD grown on Cu substrates (on 1 cm  $\times$  1 cm area). The FE properties of CNWs were measured at different temperatures so as to investigate the effect of adsorbates on the CNWs surfaces. Also, the measurements were carried out at a relatively high base pressure ( $\sim 1 \times 10^{-5}$  Torr). The FE characteristics of CNW films measured at temperatures of 20, 200, 300, and 400  $^{\circ}\text{C}$ , and at an interelectrode distance of 50  $\mu\text{m}$  are shown in Fig. 2.24. The current densities at 20  $^{\circ}\text{C}$  were 0.19 and 9.53 mA/ $\text{cm}^2$  corresponding to electric fields of 0.32 and 0.62 V/ $\mu\text{m}$ , respectively. The  $E_{10}$  obtained decreased to 0.26, 0.2, and 0.16 V/ $\mu\text{m}$ , respectively, with the temperature increasing to 200, 300, and 400  $^{\circ}\text{C}$ . The maximum  $J$  values obtained was 17.6 mA/ $\text{cm}^2$  at an applied electric field of 0.32 V/ $\mu\text{m}$  at 400  $^{\circ}\text{C}$ . The corresponding F–N plots of the FE curves are shown in Fig. 2.24b confirming that the emitted current resulted from field emission mechanism. It is to be noted that in case of measurements done at 300 and 400  $^{\circ}\text{C}$ , a perfect straight line is fitted in plots of  $\ln (J/V^2)$  versus  $1/V$ . However, the low-temperature measurements, the curve deviates from the straight line fitting particularly in the higher applied field segments (see Fig. 2.24b for 20 and 200  $^{\circ}\text{C}$ ), and therefore, F–N plots have been divided into two straight line segments. The two slopes clearly suggest that at lower temperatures there exist two energy barriers for electrons. These barriers could be caused by the adsorbates on the surface of CNWs. It was confirmed by the fact that higher field slope disappeared at higher temperatures (see Fig. 2.24b for 300 and 400  $^{\circ}\text{C}$ ). It is easy to understand that adsorbates get desorbed by heating the CNWs samples. The field enhancement factor  $\beta$  was determined to be as 31,400, 46,200, 54,800, and 62,900 for four measurements done at 20, 200, 300, and 400  $^{\circ}\text{C}$ , respectively, assuming a constant work function  $\phi$  of 5 eV. Almost threefold enhancement in  $\beta$  value for 400  $^{\circ}\text{C}$  measurements as compared to that of 20  $^{\circ}\text{C}$  one's was observed. It was found that the four lines (extrapolating the lower field curves for temperatures at 20 and 200  $^{\circ}\text{C}$ ) intersect at the same point. Based on this, it was concluded that increase in  $\beta$  value was not due to the decrease of  $\phi$  [32]. Therefore, the CNWs are superior field emitters at higher temperatures.

Similar results were also reported by Jiang et al. [112]. By using thermal desorption spectroscopy and thermal desorption mass spectroscopy, they evaluated the surface adsorbates and their desorption behaviors of CNWs. They found that the hydrocarbon materials were the main contents adsorbed on CNWs, and the absorption of  $\text{H}_2\text{O}$  and  $\text{O}_2$ , to a large degree, associated with the surface

hydrocarbon. The major species desorbed from CNW surface at 350–400 °C. CNW surface after heating in vacuum desorbs most of the surface adsorbates; CNWs exhibited the distinctly enhanced FE properties. The threshold field,  $E_{th}$ , was found 30% lower, and the emission current density increased 20 times as shown in Fig. 2.25 which shows the FE characteristics of CNWs before and after heat treatment. As discussed earlier, the larger the  $\beta$ , the higher the emission current and the CNWs usually have the equivalent height ( $h$ ) value in  $\mu\text{m}$ , while their thickness ( $d$ ) on the sharp edge tips is only  $\sim 2$  nm. Such sharp edge tips are prone to capture more adsorbates around them as they have extremely high surface energy. Even few layer adsorptions of hydrocarbons around them will strongly increase their relative thickness, resulting in a huge decrease of  $\beta$  factor and therefore the poor FE efficiency. On the other hand, if these adsorbates could be removed effectively, it will lead to a larger  $\beta$  factor enabling enhanced FE efficiency. The heating of CNWs samples certainly causes effective desorption of adsorbates and therefore was primarily accounted for the distinctly enhanced FE properties of CNWs [112].

### 2.5.3.5 Effect of Different Gas Environments for FE of CNWs

Wu et al. [32] also conducted FE measurements of CNWs under different gas environment such as  $\text{O}_2$ ,  $\text{H}_2$ ,  $\text{N}_2$ , and  $\text{CH}_4$  and observed that the FE property in  $\text{H}_2$  and  $\text{N}_2$  ambient was similar to that of in the vacuum ambient. In the presence of  $\text{O}_2$ ,

**Fig. 2.24** **a** Emission current density as a function of the electrical field at different temperatures for carbon nanowalls, and **b** the corresponding F–N plots of the curve in (a). Reproduced (Adapted) from Ref. [32] with permission of The Royal Society of Chemistry

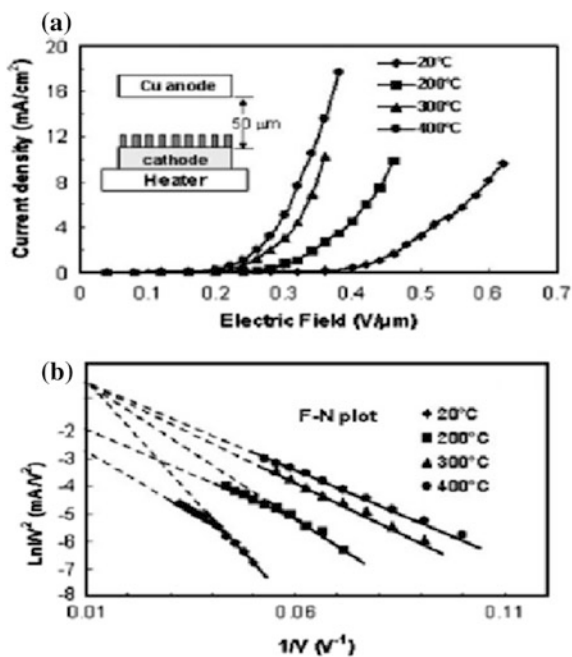
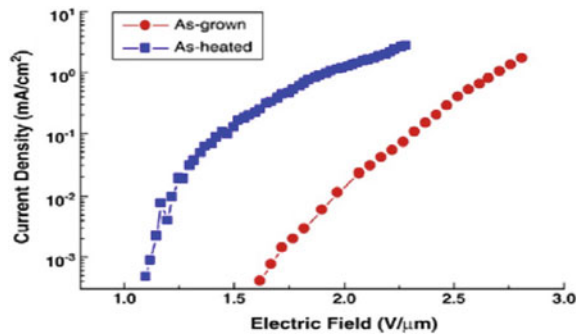


**Fig. 2.25** Field emission current curves of as-grown and as-heated CNWs. Reprinted from Ref. [112]. Copyright (2010), with permission from Elsevier



the turn-on field was higher than the vacuum condition by  $\sim >30\%$  at  $1 \text{ V}/\mu\text{m}$ . Similarly, the FE properties in  $\text{O}_2$  environment were also inferior to the results measured in  $\text{CH}_4$  environment. Emission stability was observed to degrade in  $\text{O}_2$  and  $\text{CH}_4$  ambient. Therefore, measurement environment also has strong influences on the FE properties of the CNWs.

## 2.6 Carbon Nanowalls for Energy-Related Applications

As mentioned earlier, the CNWs have large surface area and high aspect ratio and therefore have potential application in several energy harvesting applications. Few groups have successfully demonstrated variety of such applications of CNWs; a very brief summary of few of the representative work is presented below.

### 2.6.1 As Effective Electrodes in Lithium-Ion Batteries

Lithium-ion battery with high power density has been in great demands in many fields. Nanostructured materials have been recently focused a lot for the high-rate use of the battery because of their potential to provide efficient and shorter conductive path for lithium ions enabling to achieve lower internal resistivity of the electrode and hence the high power of the battery [116, 117]. Tanaike et al. [55] studied the lithium insertion behavior of CNWs by cyclic voltammetry and charge/discharge measurements. The CNWs were found to have  $>200 \text{ mAh/g}$  reversible capacities with stable charge/discharge potential. Further, the CNWs had good responses of lithium insertion/extraction reaction primarily attributing to their nanoscale and uniform size consisting of well-oriented graphene. The charge/discharge property of CNWs could be further improved by heat treatment of CNWs as heat treatment removes the by-products like amorphous carbon phase or any foreign adsorbates from CNWs surface [55]. The CNWs are also suggested as a

promising nanostructured substrate for 3-D anodes of lithium-ion batteries. Krivchenko et al. [118] showed that CNWs with sputtered silicon clusters onto them produced improved electrochemical performance which was also accounted to large surface area of freestanding CNWs and improved adhesion of silicon clusters via the SiC interface layer formation. It was proposed that the 3-D silicon-decorated CNWs had the potential to minimize the lithium diffusion length and make charge collection more effective yielding better cycling performance at high rates ( $>2000$  mAh/g) of silicon in the range of 0.05–2.00 V at 1.5 C rate [118].

### 2.6.2 As Catalyst Supports in Fuel Cells

Fuel cells, an environmentally green technology, are attracting significant interest for producing electricity by direct electrochemical conversion of hydrogen and oxygen into water [119]. Generally, platinum (Pt) nanoparticles are used as anode and cathode catalysts and carbon materials as catalyst supports. Also, the activity of a catalyst increases with the increase in the reaction surface area, therefore the diameter of catalyst particles should be as low as possible to increase the active surface area [119–122]. The support (carbon materials) for a fuel cell catalyst must have high surface area and sufficient electric conductivity for enhanced activity and efficient flow of electrons [120, 121]. Moreover, the carbon support should also have a high density of mesopores (20–40 nm region) to provide a high surface area to catalyst, to monomeric units of the Nafion ionomer and to boost the diffusion of chemical species [120, 122]. Also, any modification in electronic characteristics and geometrical dimensions of the carbon support can potentially affect the activity of the catalysts [120]. Therefore, new carbon nanostructures with unique morphology and structure have attracted much attention for the improvement of the electrochemical activity of the catalysts [120–123]. The CNWs are a potential catalyst supports owing to their unique structure, morphology, high surface area, and aspect ratio [124]. A number of groups have demonstrated application of CNWs as an effective catalysts support for Pt particles in the fuel cells. For example, Giorgi et al. [125] electrodeposited Pt nanoparticles on CNWs (grown by HF-CVD) by galvanostatic polarization to test the effectiveness of their use as electrocatalyst substrates. They found that the CNWs acted as a good substrate for Pt electrocatalyst for methanol oxidation and had remarkable enhancement as compared to standard carbon powder [125]. Machino et al. [126] demonstrated synthesis of dispersed Pt nanoparticles of 2 nm diameter on surface of CNWs by using supercritical fluid-CVD employing metal-organic compound. Similarly, Shin and coworkers [127] prepared well-dispersed Pt nanoparticle catalysts of diameter  $\sim 3$  nm supported on CNWs by a solution reduction method. The Pt/CNWs had high electrochemical active surface area and utilization, comparable to those for commercially available T-Pt/CB with good performance. Such high electrocatalytic activity was

attributed to the high electric conductivity of CNW and the improvement of electronic properties of Pt nanoparticles on the domain boundaries of CNWs, in addition to the high dispersion of Pt particles [127].

### 2.6.3 CNWs in Solar Cells

Recently, CNWs have started finding its application in solar cells also. For example, Wang et al. demonstrated that vertically aligned CNWs (they named it as carbon nanosheets, CNSs) with bi- and tri-layer graphene can be fabricated on various metal substrates from solid carbon sources by irradiation with  $H_2$  and Ar plasma. They further used few-layered CNWs by transferring them on n-Si/ $SiO_2$  to form a heterojunction solar cell and demonstrated a power conversion efficiency of 0.9% (under a simulated  $100\text{ mW/cm}^2$  AM 1.5G illumination) [128]. In this application, an n-type crystalline Si (100) wafer (resistivity:  $2\text{--}10\ \Omega\text{ cm}$ ) with 200 nm insulating  $SiO_2$  film was etched in HF solution selectively to open a window of dimension of  $3 \times 3\text{ mm}^2$ . The front and back contacts were thermally sputtered Ag on the  $SiO_2$  and Cr/Au on the back side of n-Si, respectively. Subsequently, the CNS film (1  $\mu\text{m}$  in height) was directly transferred on the top of the patterned Si wafer and was naturally dried to achieve a heterojunction solar cell. The testing of the cell was performed under a solar simulator at AM 1.5G ( $100\text{ mW/cm}^2$ ) [128]. Figure 2.26 shows the schematic of the CNS/n-Si heterojunction solar cell. The charge separation mechanism on the interface between the CNSs and the Si substrate is shown in Fig. 2.26b. The energy band diagram of the fabricated solar cell is illustrated in Fig. 2.26c and photocurrent density ( $J$ )–voltage ( $V$ ) characteristics in the dark and a  $100\text{ mW/cm}^2$  (AM 1.5 G) illumination is shown in Fig. 2.26d. The other solar cell parameters such as short circuit density ( $J_{sc}$ ), open circuit voltage ( $V_{oc}$ ), fill factor ( $FF$ ), photoconversion efficiency ( $PCE$ ), and a representative SEM image of CNSs used for solar cell are shown in the *inset* of Fig. 2.26d.

In another solar cell application of CNWs, Ho and coworkers [129] demonstrated the use of plasma-treated CNWs as counterelectrodes in dye-sensitized solar cells (DSSCs). They fabricated CNWs on a fluorine-tin-oxide (FTO) glass substrate via MPECVD using  $CH_4$  gas. Then, post-plasma treatments were performed on the CNWs in different plasma environments (using  $O_2$ ,  $H_2$ , and  $N_2$  gas) under the same conditions, after which DSSCs were fabricated using the plasma-treated CNWs as counterelectrodes. They found that photoconversion efficiency ( $PCE$ ) of the DSSC for which the as-deposited CNW was used as a counterelectrode showed an energy conversion efficiency of 1.64%, and the DSSC with the  $H_2$  post-plasma-treated CNW counterelectrode showed an energy conversion efficiency of 2.23%. Thus, the DSSC with the  $H_2$ -treated electrode presented a 36% higher efficiency than the DSSC with the as-deposited CNW electrode.

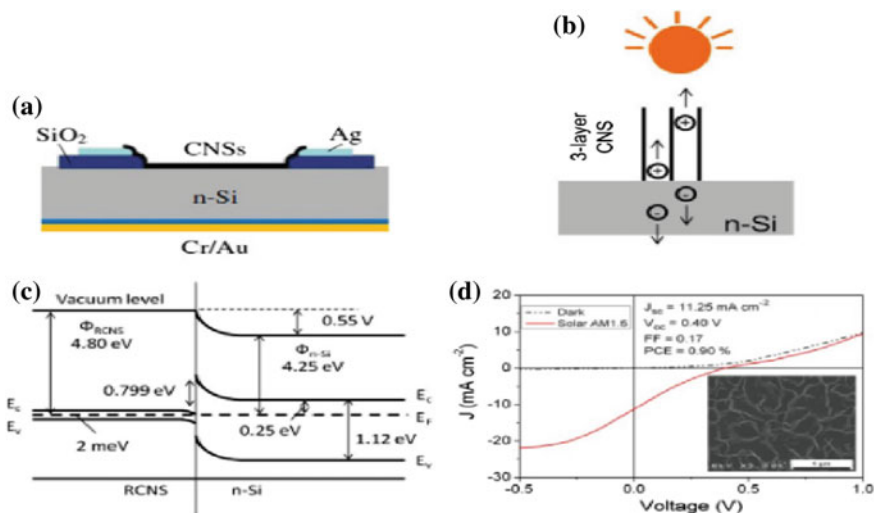


**Fig. 2.26** **a** Schematic diagram of the CNS/n-Si heterojunction solar cell, **b** illustration of the charge separation existed on the interface between the CNSs and the Si substrate, **c** the energy band diagram of the fabricated solar cell, **d**  $J$ - $V$  characteristics in the dark and under a  $100 \text{ mW cm}^{-2}$  AM 1.5 G illumination. Inset the corresponding data of  $J_{sc}$ ,  $V_{oc}$ ,  $FF$ ,  $PCE$ , and SEM image of the RCNSs used for solar cell. Reprinted from Ref. [128]. Copyright (2014), with permission from Elsevier

## 2.7 Conclusions and Future Prospects

This chapter has shown that carbon nanowalls is another, very promising class of carbon materials like graphite, diamond, C60, CNTs, or graphene. Tremendous development is made toward controlled growth of CNWs by PECVD methods. Advantage with CNWs is that their growth does not need any catalyst like the one in case of CNTs and therefore, CNWs have several advantageous features over CNTs. However, although the thickness of the nanowalls is found to be approximately few nanometers, it is difficult to control the thickness of the nanowalls with precision. Moreover, even though single layer of graphene can be obtained from the growth, present technologies and skills have not enabled us to accurately isolate the nanowall of interest. Patterned growth of CNWs is also not an easy task. Each CNW exhibits the domain structure that consists of small crystallites or nanographite domains with high degree of graphitization. Several promising applications of CNWs have been demonstrated. The CNWs are shown to be promising electron field emitters owing to high density of atomic-scale graphitic edges and good electrical conductivity. In general, excellent FE results for the CNWs are obtained; it is still too early to conclude that the CNWs could be superior to the CNTs for field emission applications. A detailed comparative and critical experiments need to be carried out under similar conditions so as to find out the real potential of the two types of nanocarbon materials as field emitter. Nevertheless,



further research has to be done to promote field emission on different substrates as well as to enhance emission reliability of CNWs.

The CNWs show quick electrochemical response for lithium insertion/extraction, which is expected for high-rate use of lithium-ion battery. Such quick response is also an evidence for small graphite domains in CNWs. In addition, the CNWs serve as catalyst support in fuel cells where Pt nanoparticles are well dispersed along the domain boundaries in CNWs. The Pt particles on the domain boundaries also exhibit relatively high electrocatalytic activity. Thus, the domain structure of CNWs is useful for negative electrodes in high-rate lithium-ion batteries and catalyst supports in fuel cells. The electrode properties might be further improved since the size of graphite domains in CNWs can be controlled by the growth condition. Such unique structure and morphology of CNWs can lead to further applications. Photovoltaic applications of CNWs have also been demonstrated though the results are preliminary but pave the way to move forward for more exciting investigations and developments in the field.

## References

1. H.W. Kroto, J.R. Heath, S.C. O'Brien, R.F. Curl, R.E. Smalley,  $C_{60}$ : buckminsterfullerene. *Nature* **318**, 162 (1985)
2. W. Kratschmer, L.D. Lamb, K. Fostiropoulos, D.R. Huffman, Solid  $C_{60}$ : a new form of carbon. *Nature* **347**, 354 (1990)
3. S. Iijima, Helical microtubules of graphitic carbon. *Nature* **354**, 56 (1991)
4. Y. Ando, X. Zhao, T. Sugai, M. Kumar, Growing carbon nanotubes. *Mater. Today* p. 22 (2004)
5. M. Inagaki, *New carbons-Control Of Structure and Functions*, 2nd edn. (Elsevier, Netherlands, 2000)
6. O.A. Shenderova, V.V. Zhirnov, D.W. Brenner, Carbon nanostructures. *Crit. Rev. Solid State Mater. Sci.* **27**, 227 (2002)
7. P.J.F. Harris, *Carbon Nanotubes and Related Structures: New Materials for the Twenty-first Century* (Cambridge University Press, UK, 1999)
8. R. Bacon, Growth, structure, and properties of graphite whiskers. *J. Appl. Phys.* **31**, 283 (1960)
9. D.E.H. Jones, *New Scientist* **32**, 245 (1966)
10. E. Osawa, *Kagaku* **25**, 854 (1970). (in Japanese)
11. D.A. Bochvar, E.G. Galperin, Huckel  $(4N + 2)$  rule and some poly-condensed systems. *Dokl. Acad. Sci. SSSR* **209**, 610 (1973)
12. S. Iijima, High resolution electron microscopy of some carbonaceous materials. *J. Microsc.* **119**, 99 (1980)
13. E.A. Rohlfing, D.M. Cox, A. Kaldor, Production and characterization of supersonic carbon clusters. *J. Chem. Phys.* **81**, 3322 (1984)
14. D. Ugarte, Curling and closure of graphitic networks under electron-beam irradiation. *Nature* **359**, 707 (1992)
15. T.W. Ebbesen, P.M. Ajayan, Large-scale synthesis of carbon nanotubes. *Nature* **358**, 220 (1992)
16. S. Iijima, T. Ichihashi, Single-shell carbon nanotubes of 1-nm diameter. *Nature* **363**, 603 (1993)

17. D.S. Bethune, C.H. Kiang, M.S. DeVries, G. Goman, R. Savoy, R. Beyers, Cobalt-catalysed growth of carbon nanotubes with single-atomic-layer walls. *Nature* **365**, 605 (1993)
18. A. Thess, R. Lee, P. Nikolaev, H. Dai, P. Petit, J. Robert, C. Xu, Y.H. Lee, S.G. Kim, A.G. Rinzler, D.T. Colbert, G.E. Scuseria, D. Tománek, J.E. Fischer, R.E. Smalley, Crystalline ropes of metallic carbon nanotubes. *Science* **273**, 483 (1996)
19. Z.F. Ren, Z.P. Huang, J.W. Wang, P. Bush, M.P. Seigal, P.N. Provencio, Synthesis of large arrays of well-aligned carbon nanotubes on glass. *Science* **282**, 1105 (1998)
20. J. Kong, H.T. Soh, A.M. Cassel, C.F. Quate, H. Dai, Synthesis of individual single-walled carbon nanotubes on patterned silicon wafers. *Nature* **395**, 878 (1998)
21. J.H. Hafner, M.J. Bronikowski, B.R. Azamian, P. Nikolaev, A.G. Rinzler, D.T. Colbert, K. A. Smith, R.E. Smalley, Catalytic growth of single-wall carbon nanotubes from metal particles. *Chem. Phys. Lett.* **296**, 195 (1998)
22. R.R. Schilttler, J.W. Seo, J.K. Gimzewski, C. Durkan, M.S.M. Saifullah, M.E. Welland, Single crystals of single-walled carbon nanotubes formed by self-assembly. *Science* **292**, 1136 (2001)
23. Y. Wu, P. Quia, T. Chong, Z. Shen, Carbon nanowalls grown by microwave plasma enhanced chemical vapor deposition. *Adv. Mater.* **14**, 64 (2002)
24. K.S. Novoselov, A.K. Geim, S.V. Morozov, D. Jiang, Y. Zhang, S.V. Dubonos, I.V. Grigorieva, A.A. Firsov, Electric field effect in atomically thin carbon films. *Science* **306**, 666 (2004)
25. J. Han, in *Carbon Nanotubes Science and Applications*, ed. by M. Meyyappan (CRC Press, Boca Raton, 2005), p. 1
26. K.B.K. Teo, C. Singh, M. Chhowalla, W.I. Milne, in *Encyclopedia of Nanoscience and Nanotechnology* ed by H.S. Nalwa, vol. 1 (American Scientific Publishers, 2004), p. 665
27. A.K. Geim, K.S. Novoselov, The rise of graphene. *Nat. Mater.* **6**, 183 (2007)
28. J.-H. Chen, C. Jang, S. Xiao, M. Ishigami, M.S. Fuhrer, Intrinsic and extrinsic performance limits of graphene devices on SiO<sub>2</sub>. *Nat. Nanotechnol.* **3**, 206 (2008)
29. A.A. Balandin, S. Ghosh, W. Bao, I. Calizo, D. Teweldebrhan, F. Miao, C.N. Lau, Superior thermal conductivity of single-layer graphene. *Nano Lett.* **8**, 902 (2008)
30. C. Lee, X. Wei, J.W. Kysar, J. Hone, Measurement of the elastic properties and intrinsic strength of monolayer graphene. *Science* **321**, 385 (2008)
31. M.D. Stoller, S. Park, Y. Zhu, J. An, R.S. Ruoff, Graphene-based ultracapacitors. *Nano Lett.* **8**, 3498 (2008)
32. Y. Wu, B. Yang, B. Zong, H. Sun, Z. Shen, Y. Feng, Carbon nanowalls and related materials. *J. Mater. Chem.* **14**, 469 (2004)
33. Y. Ando, S. Iijima, Preparation of carbon nanotubes by arc-discharge evaporation. *Jpn. J. Appl. Phys.* **32**, L107 (1993)
34. S. Iijima, T. Wakabayashi, Y. Achiba, Structures of carbon soot prepared by laser ablation. *J. Phys. Chem.* **100**, 5839 (1996)
35. Y. Ando, X. Zhao, M. Ohkohchi, Production of petal-like graphite sheets by hydrogen arc discharge. *Carbon* **35**, 153 (1997)
36. N.G. Shang, F.C.K. Au, X.M. Meng, C.S. Lee, I. Bello, S.T. Lee, Uniform carbon nanoflake films and their field emissions. *Chem. Phys. Lett.* **358**, 187 (2002)
37. S.K. Srivastava, A.K. Shukla, V.D. Vankar, Vikram Kumar, Growth, structure and field emission characteristics of petal like carbon nano-structured thin films. *Thin Solid Films* **492**, 124 (2005)
38. K. Tanaka, M. Yoshimura, A. Okamoto, K. Ueda, Growth of carbon nanowalls on a SiO<sub>2</sub> substrate by microwave plasma-enhanced chemical vapor deposition. *Jpn. J. Appl. Phys.* **44**, 2074 (2005)
39. J. Wang, T. Ito, CVD growth and field emission characteristics of nano-structured films composed of vertically standing and mutually intersecting nano-carbon sheets. *Diamond Relat. Mater.* **16**, 589 (2007)
40. A.T.H. Chuang, B.O. Boskovic, J. Robertson, Freestanding carbon nanowalls by microwave plasma-enhanced chemical vapour deposition. *Diamond Relat. Mater.* **15**, 1103 (2006)

41. A.T.H. Chuang, J. Robertson, B.O. Boskovic, K.K.K. Koziol, Three-dimensional carbon nanowall structures. *Appl. Phys. Lett.* **90**, 123107 (2007)
42. M. Hiramatsu, K. Shiji, H. Amano, M. Hori, Fabrication of vertically aligned carbon nanowalls using capacitively coupled plasma-enhanced chemical vapor deposition assisted by hydrogen radical injection. *Appl. Phys. Lett.* **84**, 4708 (2004)
43. K. Shiji, M. Hiramatsu, A. Enomoto, M. Nakamura, H. Amano, M. Hori, Vertical growth of carbon nanowalls using rf plasma-enhanced chemical vapor deposition. *Diamond and Relat. Mater.* **14**, 831 (2005)
44. M. Hiramatsu, M. Hori, Fabrication of carbon nanowalls using novel plasma processing. *Jpn. J. Appl. Phys.* **45**, 5522 (2006)
45. S. Kondo, M. Hori, K. Yamakawa, S. Den, H. Kano, M. Hiramatsu, Highly reliable growth process of carbon nanowalls using radical injection plasma-enhanced chemical vapor deposition. *J. Vacuum Sci. Techno. B* **26**, 1294 (2008)
46. T. Mori, M. Hiramatsu, K. Yamakawa, K. Takeda, M. Hori, Fabrication of carbon nanowalls using electron beam excited plasma-enhanced chemical vapor deposition. *Diamond Relat. Mater.* **17**, 1513 (2008)
47. J. Wang, M. Zhu, R.A. Outlaw, X. Zhao, D.M. Manos, B.C. Holloway, Synthesis of carbon nanosheets by inductively coupled radio-frequency plasma enhanced chemical vapor deposition. *Carbon* **42**, 2867 (2004)
48. M. Zhu, J. Wang, R.A. Outlaw, K. Hou, D.M. Manos, B.C. Holloway, Synthesis of carbon nanosheets and carbon nanotubes by radio frequency plasma enhanced chemical vapor deposition. *Diamond Relat. Mater.* **16**, 196 (2007)
49. J.J. Wang, M.Y. Zhu, R.A. Outlaw, X. Zhao, D.M. Manos, B.C. Holloway, V.P. Mammana, Free-standing subnanometer graphite sheets. *Appl. Phys. Lett.* **85**, 1265 (2004)
50. G. Sato, T. Morio, T. Kato, R. Hatakeyama, Fast growth of carbon nanowalls from pure methane using helicon plasma-enhanced chemical vapor deposition. *Jpn. J. Appl. Phys.* **45**, 5210 (2006)
51. H.G. Jain, H. Karacuban, D. Krix, H.W. Becker, H. Nienhaus, V. Buck, Carbon nanowalls deposited by inductively coupled plasma enhanced chemical vapor deposition using aluminum acetylacetonate as precursor. *Carbon* **49**, 4987 (2011)
52. A. Yoshimura, S. Kurita, M. Tachibana, K. Kojima, P.M. Morales, H. Nakai, Fabrication of carbon nanowalls by dc plasma-enhanced chemical vapor deposition and characterization of their structures, *Proceedings of 2005 5th IEEE Conference on Nanotechnology Nagoya, Japan* (2005)
53. S. Kurita, A. Yoshimura, H. Kawamoto, T. Uchida, K. Kojima, M. Tachibana, P. Molina-Morales, H. Nakai, Raman spectra of carbon nanowalls grown by plasma-enhanced chemical vapor deposition. *J. Appl. Phys.* **97**, 104320 (2005)
54. K. Kobayashi, M. Tanimura, H. Nakai, Nanographite domains in carbon nanowalls. *J. Appl. Phys.* **101**, 094306 (2007)
55. O. Tanaike, N. Kitada, H. Yoshimura, H. Hatori, K. Kojima, M. Tachibana, Lithium insertion behavior of carbon nanowalls by dc plasma CVD and its heat-treatment effect. *Solid State Ionics* **180**, 381 (2009)
56. Z. Bo, K. Yu, G. Lu, P. Wang, S. Mao, J. Chen, Understanding growth of carbon nanowalls at atmospheric pressure using normal glow discharge plasma-enhanced chemical vapor deposition. *Carbon* **49**, 1849 (2011)
57. H. Yoshimura, S. Yamada, A. Yoshimura, I. Hirose, K. Kojima, M. Tachibana, Grazing incidence X-ray diffraction study on carbon nanowalls. *Chem. Phys. Lett.* **482**, 125 (2009)
58. T. Itoh, S. Shimabukuro, S. Kawamura, S. Nonomura, Preparation and electron field emission of carbon nanowall by Cat-CVD. *Thin Solid Films* **501**, 314 (2006)
59. N. Lisi, R. Giorgi, M. Re, Carbon nanowall growth on carbon paper by hot filament chemical vapour deposition and its microstructure. *Carbon* **49**, 2134 (2011)
60. R.J. Nemanich, S.A. Solin, First- and second-order Raman scattering from finite-size crystals of graphite. *Phys. Rev. B* **20**, 392 (1979)

61. J. Yu, Q. Zhang, J. Ahn, S.F. Yoon, Y.J. Rusli, B. Li, K. Gan, K.H. Tan Chew, Synthesis of carbon nanostructures by microwave plasma chemical vapor deposition and their characterization. *Mater. Sci. Eng. B* **90**, 16 (2002)
62. F. Tuinstra, J.L. Koenig, Raman spectrum of graphite. *J. Chem. Phys.* **53**, 1126 (1970)
63. A.C. Ferrari, J. Robertson, Interpretation of Raman spectra of disordered and amorphous carbon. *Phys. Rev. B* **61**, 14095 (2000)
64. A.C. Ferrari, J. Robertson, Resonant Raman spectroscopy of disordered, amorphous, and diamond like carbon. *Phys. Rev. B* **64**, 075414 (2001)
65. H. Wang, Y. Wu, C.K.S. Choong, J. Zhang, K.L. Teo, Z. Ni, Z. Shen, Disorder induced bands in first order Raman spectra of carbon nanowalls, *Nanotechnology*, 2006. IEEE-NANO 2006. Sixth IEEE Conference, vol. 1, pp. 219–222
66. Z.H. Ni, H.M. Fan, X.F. Fan, H.M. Wang, Z. Zheng, Y.P. Feng, Y.H. Wu, Z.X. Shen, High temperature Raman spectroscopy studies of carbon nanowalls. *J. Raman Spectrosc.* **38**, 1449 (2007)
67. Y. Wu, B. Yang, Effects of localized electric field on the growth of carbon nanowalls *Nano Lett.* **2**, 355 (2002)
68. B. Chapman, *Glow Discharge Process* (Wiley, New York, 1980)
69. C. Bower, W. Zhu, S. Jin, O. Zhou, Plasma-induced alignment of carbon nanotubes. *Appl. Phys. Lett.* **77**, 830 (2000)
70. M. Zhu, J. Wang, B.C. Holloway, R.A. Outlaw, X. Zhao, K. Hou, V. Shutthanandan, D.M. Manos, A mechanism for carbon nanosheet formation. *Carbon* **45**, 2229 (2007)
71. I. Levchenko, K. Ostrikov, A.E. Rider, E. Tam, S.V. Vladimirov, S. Xu, Growth kinetics of carbon nanowall-like structures in low-temperature plasmas. *Phys. Plasmas* **14**, 063502 (2007)
72. R.H. Fowler, L.W. Nordheim, Electron emission in intense electric fields. *Proc. R. Soc. London A* **119**, 173 (1928)
73. Y. Cheng, O. Zhou, Electron field emission from carbon nanotubes. *C.R. Physique* **4**, 1021 (2003)
74. Z.P. Huang, Y. Tu, D.L. Carnahan, Z.F. Ren, in *Encyclopedia of Nanoscience and Nanotechnology* ed. by H.S. Nalwa, vol. 3 (American Scientific Publishers, 2004), p. 401
75. P. Gröning, L. Nilsson, P. Ruffieux, R. Clergereaux, O. Gröning, in *Encyclopedia of Nanoscience and Nanotechnology*, ed. by H.S. Nalwa, vol. 1 (American Scientific Publishers, 2004), p. 547
76. W. Zhu, C. Bower, G.P. Kochanski, S. Jin, Electron field emission from nanostructured diamond and carbon nanotubes. *Solid-State Electron* **45**, 921 (2001)
77. C.A. Spindt, A thin-film field-emission cathode. *J. Appl. Phys.* **39**, 3504 (1968)
78. A.G. Rinzler, J.H. Hafner, P. Nikolaev, L. Lou, S.G. Kim, D. Tomanek, P. Nordlander, D.T. Colbert, R.E. Smalley, Unraveling nanotubes: field emission from an atomic wire. *Science* **269**, 1550 (1995)
79. W.A. de Heer, A. Châtelain, D. Ugarte, A carbon nanotube field-emission electron source. *Science* **270**, 1179 (1995)
80. P.G. Collins, A. Zettl, A simple and robust electron beam source from carbon nanotubes. *Appl. Phys. Lett.* **69**, 1969 (1996)
81. P.G. Collins, A. Zettl, Unique characteristics of cold cathode carbon-nanotube-matrix field emitters. *Phys. Rev. B* **55**, 9391 (1997)
82. Y. Saito, K. Hamaguchi, K. Hata, K. Uchida, Y. Tasaka, F. Ikazaki, M. Yumura, A. Kasuya, Y. Nishina, Conical beams from open nanotubes. *Nature* **389**, 554 (1997)
83. Q.H. Wang, T.D. Corrigan, J.Y. Dai, R.P.H. Chang, A.R. Krauss, Field emission from nanotube bundle emitters at low fields. *Appl. Phys. Lett.* **70**, 3308 (1997)
84. J.M. Bonard, F. Maier, T. Stoeckli, A. Chatelain, W.A. de Heer, J.P. Salvetat, L. Forro, Field emission properties of multiwalled carbon nanotubes. *Ultramicroscopy* **73**, 7 (1998)
85. S. Fan, M.G. Chapline, N.R. Franklin, T.W. Tombler, A.M. Cassell, H. Dai, Self-oriented regular arrays of carbon nanotubes and their field emission properties. *Science* **283**, 512 (1999)

86. O.M. Kuttel, O. Groening, C. Emmenegger, L. Schlapbach, Electron field emission from phase pure nanotube films grown in a methane/hydrogen plasma. *Appl. Phys. Lett.* **73**, 2113 (1998)
87. Y. Saito, S. Uemura, Field emission from carbon nanotubes and its application to electron sources. *Carbon* **38**, 169 (2000)
88. M. Chhowalla, C. Ducati, N.L. Rupesinghe, K.B.K. Teo, G.A.J. Amaratunga, Field emission from short and stubby vertically aligned carbon nanotubes. *Appl. Phys. Lett.* **79**, 2079 (2001)
89. K.B.K. Teo, M. Chhowalla, G.A.J. Amaratunga, W.I. Milne, G. Pirio, P. Legagneux, F. Wyczisk, D. Pribat, D.G. Hasko, Field emission from dense, sparse, and patterned arrays of carbon nanofibers. *Appl. Phys. Lett.* **80**, 2011 (2002)
90. S.H. Jo, Y. Tu, Z.P. Huang, D.L. Carnahan, D.Z. Wang, Z.F. Ren, Effect of length and spacing of vertically aligned carbon nanotubes on field emission properties. *Appl. Phys. Lett.* **82**, 3520 (2003)
91. S.H. Jo, Y. Tu, Z.P. Huang, D.L. Carnahan, J.Y. Huang, D.Z. Wang, Z.F. Ren, Correlation of field emission and surface microstructure of vertically aligned carbon nanotubes. *Appl. Phys. Lett.* **84**, 413 (2004)
92. S.K. Srivastava, V.D. Vankar, D.V. Sridhar Rao, V. Kumar, Enhanced field emission characteristics of nitrogen-doped carbon nanotube films grown by microwave plasma enhanced chemical vapor deposition process. *Thin Solid Films* **515**, 1851 (2006)
93. S.K. Srivastava, V.D. Vankar, V. Kumar, Excellent field emission properties of short conical carbon nanotubes prepared by microwave plasma enhanced CVD process. *Nanoscale Res. Lett.* **3**, 25 (2008)
94. S.K. Srivastava, V.D. Vankar, V. Kumar, Effect of catalyst film thickness on the growth, microstructure and field emission characteristics of carbon nanotubes. In *Physics of Semiconductor Devices, 2007. IWPSD 2007. International Workshop on, Physics of Semiconductor Devices, 2007. IWPSD 2007. International Workshop on*, pp. 836–839, IEEE
95. S. Chhoker, S.K. Srivastava, V.D. Vankar, Field emission properties of carbon nanostructures: a review, physics of semiconductor devices, 2007. IWPSD 2007. International Workshop on, Physics of Semiconductor Devices, 2007. IWPSD 2007. International Workshop on, pp. 820–826, IEEE
96. S.K. Srivastava, V.D. Vankar, V. Kumar, V.N. Singh, Effect of substrate morphology on growth and field emission properties of carbon nanotube films. *Nanoscale Res. Lett.* **3**, 205 (2008)
97. H. Sharma, V. Kaushik, P. Girdhar, V.N. Singh, A.K. Shukla, V.D. Vankar, Enhanced electron emission from titanium coated multiwalled carbon nanotubes. *Thin Solid Films* **518**, 6915 (2010)
98. Y. Saito, K. Hamaguchi, T. Nishino, K. Hata, K. Tohji, A. Kasuya, Y. Nishina, Field emission patterns from single-walled carbon nanotubes. *Jpn. J. Appl. Phys.* **36**, L1340 (1997)
99. J.-M. Bonard, J.-P. Salvetat, T. Stockli, W.A. de Heer, L. Forro, A. Châtelain, Field emission from single-wall carbon nanotube films. *Appl. Phys. Lett.* **73**, 918 (1998)
100. W.B. Choi, D.S. Chung, J.H. Kang, H.Y. Kim, Y.W. Jin, I.T. Han, Y.H. Lee, J.E. Jung, N.S. Lee, G.S. Park, J.M. Kim, Fully sealed, high-brightness carbon-nanotube field-emission display. *Appl. Phys. Lett.* **75**, 3129 (1999)
101. W. Zhu, C. Bower, O. Zhou, G. Kochanski, S. Jin, Large current density from carbon nanotube field emitters. *Appl. Phys. Lett.* **75**, 873 (1999)
102. S.M. Sze, *VLSI Technology* (McGraw Hill, New York, 1988), p. 309
103. J. Wang, T. Ito, Improved field emission characteristics of nano-structured carbon films deposited on polycrystalline CVD diamond. *Diam. Relat. Mater.* **16**, 364–368 (2007)
104. E. Stratakis, R. Giorgi, M. Barberoglou, Th Dikonimos, E. Salernitano, N. Lisi, E. Kymakis, Three-dimensional carbon nanowall field emission arrays. *Appl. Phys. Lett.* **96**, 043110 (2010)

105. W. Takeuchi, H. Kondo, T. Obayashi, M. Hiramatsu, M. Hori, Electron field emission enhancement of carbon nanowalls by plasma surface nitridation. *Appl. Phys. Lett.* **98**, 123107 (2011)
106. Y. Tzeng, C.-L. Chen, Y.-Y. Chen, C.-Y. Liu, Carbon nanowalls on graphite for cold cathode applications. *Diamond & Relat. Mater.* **19**, 201 (2010)
107. P.H. Talemi, G.P. Simon, Field emission study of graphene nanowalls prepared by microwave-plasma method. *Carbon* **49**, 2875 (2011)
108. M.Y. Zhu, R.A. Outlaw, M. Bagge-Hansen, H.J. Chen, D.M. Manos, Enhanced field emission of vertically oriented carbon nanosheets synthesized by  $C_2H_2/H_2$  plasma enhanced CVD. *Carbon* **49**, 2526 (2011)
109. S.A. Evlashin, Y.A. Mankelevich, V.V. Borisov, A.A. Pilevskii, A.S. Stepanov, Victor A. Krivchenko, N.V. Suetin, A.T. Rakhimov, Emission properties of carbon nanowalls on porous silicon. *J. Vac. Sci. Technol. B* **30**, 021801 (2012)
110. S. Shimada, K. Teii, M. Nakashima, Low threshold field emission from nitrogen-incorporated carbon nanowalls. *Diamond & Relat. Mater.* **19**, 956 (2010)
111. A. Malesevic, R. Kemps, A. Vanhulsel, M.P. Chowdhury, A. Volodin, C.V. Haesendonck, Field emission from vertically aligned few-layer graphene. *J. Appl. Phys.* **104**, 084301 (2008)
112. N. Jiang, H.X. Wang, H. Sasaoka, T. Deno, K. Nishimura, Thermal desorption and its effects on field emission properties of carbon nanowalls. *Mater. Lett.* **64**, 2025 (2010)
113. S. Chhoker, S.K. Arora, P. Srivastava, V.D. Vankar, Electron field emission from graphitic nanoflakes grown over vertically aligned carbon nanotubes. *J. Nanosci. Nanotech.* **8**, 4309 (2008)
114. V. Kaushik, A.K. Shukla, V.D. Vankar, Microwave plasma CVD-grown graphene–CNT hybrids for enhanced electron field emission applications. *Appl. Phys. A* **117**, 2197 (2014)
115. V. Kaushik, A.K. Shukla, V.D. Vankar, Improved electron field emission from metal grafted graphene composites. *Carbon* **62**, 337 (2015)
116. P.R. Bueno, E.R. Leite, Nanostructured Li ion insertion electrodes. 1. Discussion on fast transport and short path for ion diffusion. *J. Phys. Chem. B* **107**, 8868 (2003)
117. L. Taberna, S. Mitra, P. Poizot, P. Simon, J.M. Tarascon, *Nature Mater.* **5**, 567 (2006)
118. V.A. Krivchenko, D.M. Itkis, S.A. Evlashin, D.A. Semenenko, E.A. Goodilin, A.T. Rakhimov, A.S. Stepanov, N.V. Suetin, A.A. Pilevsky, P.V. Voronin, Carbon nanowalls decorated with silicon for lithium-ion batteries. *Carbon* **50**, 1422 (2012)
119. J. Larminie, A. Dicks, *Fuel Cell Systems Explained*, 2nd edn. (John Wiley & Sons, New York, 2003)
120. E. Antolini, Carbon supports for low-temperature fuel cell catalysts. *Appl. Catal. B: Environ.* **88**, 1 (2009)
121. A.L. Dicks, The role of carbon in fuel cells. *J. Power Sources* **156**, 128 (2006)
122. S.H. Joo, S.J. Choi, I. Oh, J. Kwak, Z. Liu, O. Terasaki, R. Ryoo, Ordered nanoporous arrays of carbon supporting high dispersions of platinum nanoparticles. *Nature* **412**, 169 (2001)
123. T.W. Kim, I.S. Park, R. Ryoo, A synthetic route to ordered mesoporous carbon materials with graphitic pore walls. *Angew Chem. Int. Ed.* **42**, 4375 (2003)
124. M. Tachibana, in *Structural Characterization of Carbon Nanowalls and Their Potential Applications in Energy Devices* (Chapter 6). *Book: Two-Dimensional Carbon: Fundamental Properties, Synthesis, Characterization, and Applications*, ed. by Yihong Wu, Zexiang Shen, and Ting Yu, Copyright © 2014 Pan Stanford Publishing Pte. Ltd., pp. 121–152
125. L. Giorgi, T.D. Makris, R. Giorgi, N. Lisi, E. Salernitano, Electrochemical properties of carbon nanowalls synthesized by HF-CVD. *Sens. Actuators B: Chemical* **126**, 144 (2007)
126. T. Machino, W. Takeuchi, H. Kano, M. Hiramatsu, M. Hori, Carbon nanostructures with an ultrahigh aspect ratio employing supercritical fluid chemical vapor deposition process. *Appl. Phys. Express* **2**, 025001 (2009)



127. S.C. Shin, A. Yoshimura, T. Matsuo, M. Mori, M. Tanimura, A. Ishihara, K. Ota, M. Tachibana, Carbon nanowalls as platinum support for fuel cells. *J. Appl. Phys.* **110**, 104308 (2011)
128. Z. Wang, M. Shoji, K. Baba, T. Ito, H. Ogata, Microwave plasma-assisted regeneration of carbon nanosheets with bi- and trilayer of graphene and their application to photovoltaic cells. *Carbon* **67**, 326 (2014)
129. Y.H. Jung, W.S. Choi, B. Hong, Post-plasma treatment of a carbon nanowall for use as a counter electrode in a dye-sensitized solar cell. *J Korean Phys. Soc.* **65**, 291 (2014)

<http://www.springer.com/978-981-10-6213-1>

Nanomaterials and Their Applications

Khan, Z.H. (Ed.)

2018, XIII, 321 p. 195 illus., 110 illus. in color.,

Hardcover

ISBN: 978-981-10-6213-1